

THESIS FOR THE DEGREE OF DOCTOR OF PHILOSOPHY

Development of Multi-grit cBN  
Grinding Wheel for Crankshaft Grinding

NASTJA MACEROL

Department of Industrial and Materials Science

CHALMERS UNIVERSITY OF TECHNOLOGY

Gothenburg, Sweden 2022

Development of Multi-grit cBN Grinding Wheel for Crankshaft Grinding

NASTJA MACEROL

ISBN 978-91-7905-771-8

© NASTJA MACEROL, 2022.

Doktorsavhandlingar vid Chalmers tekniska högskola

Ny serie nr 5237

ISSN 0346-718X

Department of Industrial and Materials Science

Chalmers University of Technology

SE-412 96 Gothenburg

Sweden

Telephone + 46 (0)31-772 1000

Printed by Chalmers Reproservice

Gothenburg, Sweden 2022

# Development of Multi-grit cBN Grinding Wheel for Crankshaft Grinding

Nastja Macerol

Department of Industrial and Materials Science  
Chalmers University of Technology

## Abstract

A crankpin, part of a crankshaft, has a complex profile that is difficult to grind. The process often causes challenges such as excessive heat on the crankpin sidewall and wheel wear on the radius, causing reduced dressing interval. Different solutions were proposed to overcome these challenges, mainly focusing on the process, i.e. grinding strategies. However, the work presented in this thesis is concerned with optimising the superabrasive grinding wheel.

A novel analytical assessment framework was developed for evaluating grinding wheel performance that can account for the effects of grit properties and dressing conditions on the wheel topography and, in turn, grinding performance. Based on the model of cutting and sliding grinding force components, a set of performance indicators were derived and then used to evaluate the effect of the wheel topography on the grinding process. Results showed that grit toughness, thermal stability, size and concentration affect the intrinsic specific grinding energy via grit protrusion and sliding component via wear flat area. On the other hand, the grit shape only affects the wear flat area but maintains the intrinsic specific grinding energy regardless if the grit has a higher or lower aspect ratio (blockier or elongated).

To complement grinding performance information, wear was evaluated via grinding and lapping tests. The analyses revealed that wheels containing grits with a higher aspect ratio (elongated grits), lower toughness, lower concentration, or smaller size generate lower grinding forces; however, they wore faster. On the other hand, wheels featuring grits with a lower aspect ratio (blocky grits), higher toughness, higher concentration or coarser grit had the opposite effect. They generated higher forces and wore slower, exhibiting longer tool life.

Findings from laboratory-based trials resulted in two crankpin wheel designs. One aimed to reduce heat generation, while the other targeted less wheel wear. Industrial tests at the end user demonstrated that the favourable design contained elongated and smaller grits at a lower concentration, because it reduced heat generation despite the higher wheel wear. This was confirmed via the Barkhausen noise measurements, which showed a 20% reduction in intensity compared to the reference wheel and a 30% reduction in intensity compared to the wheel design containing blockier and larger grit at higher concentration.

**Keywords:** automotive, crankshaft, grinding, cubic Boron Nitride, grinding wheels, grit shape, grit size, grit toughness, grit concentration, wear



## Preface

This thesis is based on the work performed at Element Six (UK) Ltd Global Innovation Centre and Scania CV AB under the supervision of Prof. Peter Krajnik, Dr Luiz Franca (industrial supervisor) and Dr Radovan Drazumeric (co-supervisor) of the University of Ljubljana. The work has been carried out in part within the ‘CRANK-WHEEL’ project funded by Scania CV AB, Element Six (UK) Ltd. and Tyrolit - Schleifmittelwerke Swarovski AG & Co K.G.

The thesis consists of an introductory part and the following appended papers:

- Paper I:       **A methodology for the evaluation of CBN abrasive grits**  
Nastja Macerol, Luiz Franca, Wayne Leahy, Paul White and Peter Krajnik  
*Proceedings of the 19<sup>th</sup> International Symposium on Advances in Abrasive Technology, Stockholm, Sweden, 2016*
- Paper II:       **Superabrasive applications in grinding of crankshafts: A review**  
Nastja Macerol, Luiz Franca, Wayne Leahy and Peter Krajnik  
*Proceedings of the 20<sup>th</sup> International Symposium on Advances in Abrasive Technology, Okinawa, Japan, 2017*
- Paper III:       **Effect of the grit shape on the performance of vitrified-bonded cBN grinding wheel**  
Nastja Macerol, Luiz F.P. Franca and Peter Krajnik  
*Journal of Materials Processing Technology, 2020; 277:1-9*
- Paper IV:       **A lapping-based test method to investigate wear behaviour of bonded-abrasive tools**  
Nastja Macerol, Luiz Franca, Helmi Attia and Peter Krajnik  
*CIRP Annals, 2022; 71(1):305-308*
- Paper V:       **The effects of grit properties and dressing on grinding mechanics and wheel performance: Analytical assessment framework**  
Nastja Macerol, Luiz Franca, Radovan Drazumeric and Peter Krajnik  
*International Journal of Machine Tools and Manufacture, 2022, 180:1-13*
- Paper VI:       **Development of multi-grit cBN grinding wheel for crankshaft grinding: Effects of grit types on specific energy, wheel wear and surface integrity**  
Nastja Macerol, Luiz Franca, Radovan Drazumeric, Roope Roininen and Peter Krajnik  
*To be submitted to the Journal of Materials Processing Technology*

## **Contribution to the appended papers**

- Paper I: I conceptualised, planned and oversaw testing followed by data curation and investigation. I also wrote the draft of the paper. Co-authors did the review and editing. The resources were provided by E6.
- Paper II: I did the research and wrote the draft of the review paper. Co-authors did the review and editing.
- Paper III: Together with Dr Luiz Franca, we planned conceptualisation. I designed and oversaw testing and curated and evaluated the data. I also wrote the first draft while co-authors did the review and editing. The resources were provided by E6.
- Paper IV: All authors contributed to conceptualisation. I planned and oversaw testing, and curated and evaluated data. I wrote the first draft. The review and editing were done by co-authors. The resources were provided by E6.
- Paper V: All authors planned conceptualisation and methodology. I designed and oversaw testing and conducted imaging and analysis of grinding wheels. I also curated and evaluated data and wrote the draft with the help from Dr Luiz Franca. Co-authors did the review and editing. The resources were provided by E6.
- Paper VI: All authors contributed to conceptualisation and methodology. Roope Roininen did testing with my support (virtual discussions for next steps). I did data curation and evaluation with subsequent support from Dr Radovan Drazumeric. I will finalise the draft, and co-authors will review and edit the work. The resources were provided by Scania.

# Contents

1	Introduction .....	1
1.1	Industrial challenges in crankshaft grinding .....	1
1.2	Research objective.....	3
1.2.1	Research approach and limitations.....	3
2	Background and state-of-the-art.....	5
2.1	Crankpin grinding strategies: radial and angular plunge methods .....	5
2.2	Crankpin grinding strategies developed by machine builders .....	6
2.3	Dressing strategies.....	8
2.4	Grinding wheel.....	9
2.4.1	Vitrified bond system .....	9
2.4.2	Porosity.....	10
2.4.3	Cubic Boron Nitride (cBN) abrasive grit .....	11
2.4.4	State-of-the-art in crankpin grinding wheel designs .....	13
3	New crankpin grinding wheel development.....	15
3.1	Grit properties and characterisation .....	15
3.2	Analytical assessment framework for evaluation of grinding wheel performance ..	18
3.3	Laboratory tests to evaluate grit performance.....	21
3.3.1	Grinding tests .....	22
3.3.1.1	Window of operation test (minimum wheel wear).....	22
3.3.1.2	Wear test.....	22
3.3.2	A lapping-based test method .....	23
3.4	Results and discussion.....	24
3.4.1	Grit shape (aspect ratio- AR) effects on grinding performance.....	24
3.4.2	Grit concentration effects on grinding performance .....	27
3.4.3	Evaluation of effects of grit size.....	29
3.5	Wear rate in accelerated tests using lapping-based test method .....	32
3.5.1	Wear trends observed in lapping and grinding trials.....	33

3.6	Crankshaft grinding wheel design .....	34
3.7	Grinding wheel prototypes .....	34
4	Production trials .....	37
4.1	Test setup.....	37
4.2	Process evaluation .....	38
4.3	Results and discussion.....	40
5	Summary and future work.....	47
5.1	Proposed solution and suggestions for future work .....	48
5.2	Scientific contributions .....	49
6	Acknowledgements .....	50
7	References .....	51



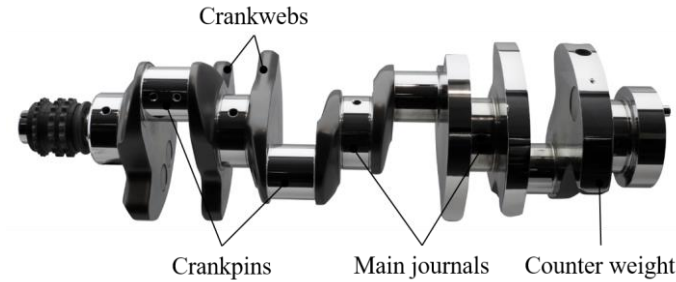




# 1 Introduction

## 1.1 Industrial challenges in crankshaft grinding

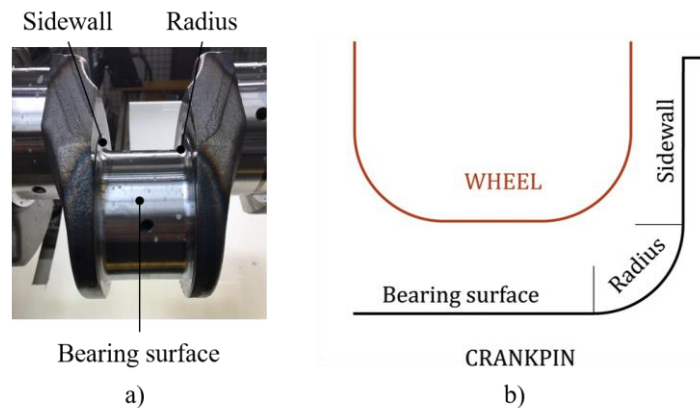
The crankshaft is a crucial mechanical part of an internal combustion engine that converts reciprocating motion into rotation motion. A typical crankshaft consists of crankpins or ‘pins’, crankwebs, balancing weights, and main journals, see Fig. 1.



**Fig. 1.** Parts of a crankshaft (Adopted and modified with permission from Element Six, (UK), Ltd).

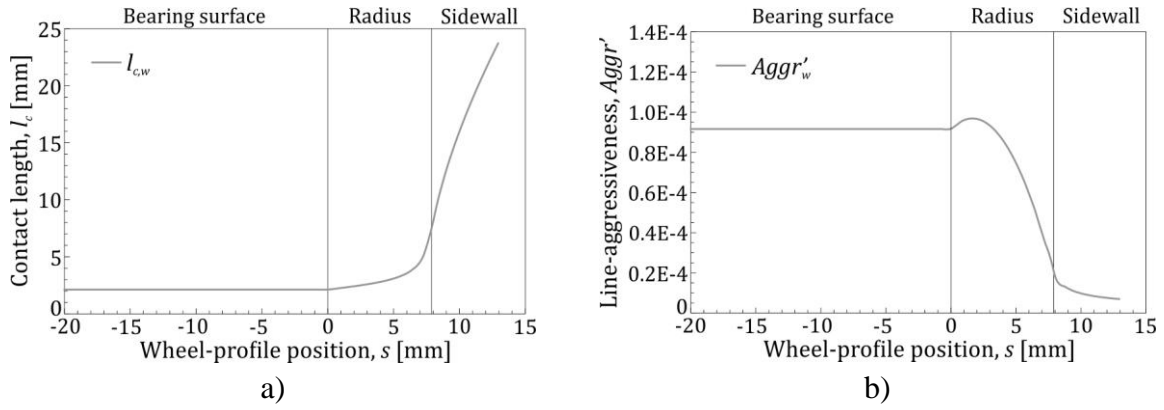
The finishing of crankshafts is challenging due to the stringent surface integrity requirements and geometrical features posed by design and performance demands. Crankshafts for heavy-duty diesel engines are typically forged, soft machined, induction hardened and finally ground at the end of the manufacturing chain. Subsequently, the ground bearing surfaces are then superfinished (using stone and/or tape) [1]. The cost associated with the grinding process to achieve surface integrity demands is high. Any improvements to reduce cost, cycle time and make the operation more productive without affecting the crankshaft quality is welcome.

The profile of crankpins (see Fig. 2a) is particularly challenging to grind. Generally, crankpins are set eccentrically to the shaft centreline, and the grinding process needs to machine three distinct sections: (i) cylindrical bearing surface, (ii) radius and (iii) sidewall (see Fig. 2b).



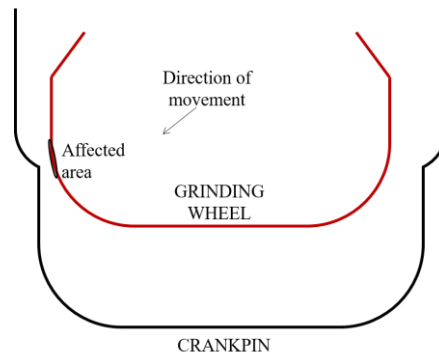
**Fig. 2.** a) Detailed crankpin view and b) sketch of crankpin grinding (Reprinted from [2], with permission from Elsevier).

The cylindrical grinding of the bearing surface is not particularly problematic. However, grinding of the crankpin's sidewall is challenging due to heat generation and, consequently, surface integrity issues [3]. Results from the crankpin grinding process modelled by Drazumeric et al. [4] suggest that the side wall is subjected to a large contact length (Fig. 3a) and very low aggressiveness<sup>1</sup> (Fig. 3b), causing a predominantly rubbing mechanism. This rubbing process increases heat, leading to thermal damage on the side wall.



**Fig. 3.** Modelled grinding conditions for crankpin grinding across its profile: a) contact length and b) line aggressiveness [4].

The second challenge is the uneven wear of the grinding wheel. Wheels in production at Scania have shown localised wheel wear at the transition section between the wheel radius and side wall (radius-side wall interface), see Fig. 4. From the grinding wheel perspective, this section removes more material and is exposed to higher aggressiveness. The excessive wheel wear at the radius-sidewall interface can shorten the dressing time interval, on the one hand increasing the tool costs and the overall crankshaft manufacturing cost on the other hand.



**Fig. 4.** Localised grinding wheel wear on the radius and side wall transition.

Critical wheel wear or thermal damage of the workpiece typically require wheel dressing, which consequently define the dressing interval. Over the past 40 years, different solutions have been considered to improve the dressing cycle [5–9]. These solutions can be divided into two groups: (i) grinding process strategy and (ii) set-up improvements. The work presented in this thesis

<sup>1</sup> A dimensionless parameter proportional to the undeformed maximum chip thickness [15].

aimed to improve grinding set-up components, more precisely, the grinding wheel design to increase dressing interval.

## **1.2 Research objective**

The ultimate research goal was to develop a new grinding wheel that would increase the dressing interval of the crankshaft grinding process. The work was done in collaboration with the International Grinding Institute (IGI), Element Six (UK) Ltd. (E6), Tyrolit - Schleifmittelwerke Swarovski AG & Co K.G and the end user Scania CV AB. Each stakeholder supported the project by supplying crucial requirements specifications regarding workpiece geometrical and surface integrity, grinding wheel geometry/specification and grinding/dressing process details. Tyrolit also produced customised grinding wheels with E6 unique cBN grits. Laboratory tests were conducted at E6 and production trials at Scania.

Work focused on developing the knowledge of how the wheel performance can be modified by changing wheel design, particularly grit properties. The following research questions set at the beginning of the project were followed up in the implementation of work and this thesis:

1. Can the wheel performance be modified by changing the wheel design?
2. Which grit properties affect grinding performance and how?
3. How should the crankshaft grinding wheel be designed to tackle industrial challenges?
4. Compared to the reference wheel, how much can the crankshaft grinding process be improved with a customised wheel design?

### **1.2.1 Research approach and limitations**

The research approach is presented in Fig. 5. Initially, an extensive literature review and discussions with stakeholders were conducted to develop an understanding of different crankshaft grinding strategies and grinding/dressing set-ups and the current grinding wheel solutions. Then, the project scope was refined, including different work packages from theory/fundamentals to production trials at Scania. Several tests were also conducted in the laboratory to assess the performance of different customised grits produced by E6. Based on the grits evaluation and understanding of the process, two grinding wheels were designed, fabricated and tested alongside the reference wheel, typically used in production at Scania.

The thesis was limited to the grinding wheel investigation, principally the effects of grit properties and concentration on heat generation and wheel wear. The bond properties and the grinding set-up in the laboratory and production-based trials were kept constant. Due to time restrictions in production, only one dressing interval per grinding wheel was considered, i.e. grinding 15 crankshafts per dressing interval. To limit the source of variation, workpiece material from a single supplier and one specific machine tool were utilised for all tests.

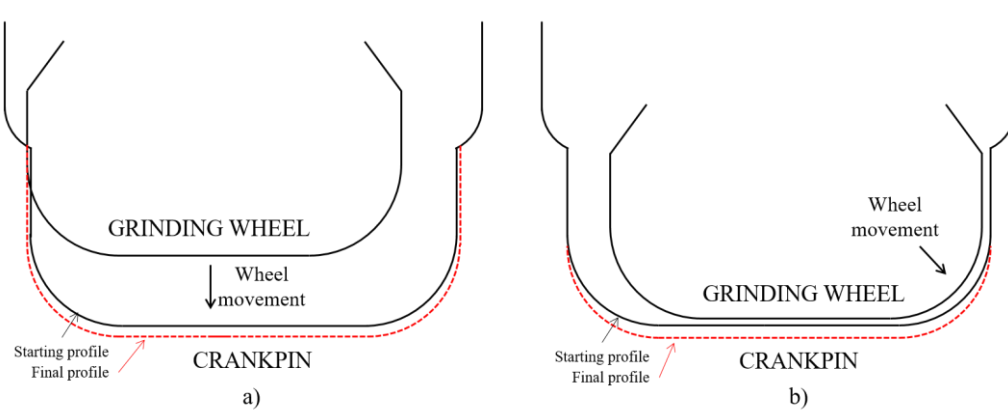


## 2 Background and state-of-the-art

An extensive literature review was conducted to learn about the crankpin grinding process and strategies to improve the dressing interval. This study further provided information about the proprietary solutions disclosed in patents, refined the focus, and helped in identifying the research questions.

### 2.1 Crankpin grinding strategies: radial and angular plunge methods

The most common process used for crankpin grinding is radial plunge during roughing operation followed by angle plunge during the finishing process [2]. In radial plunge grinding [7], the grinding wheel is plunging radially from the outmost diameter of the crankpin to the innermost diameter at the end of the cycle [10]; see Fig. 6a. The part of the radius that initially starts grinding the side wall does most of the material removal under aggressive conditions. This can lead to localized wear, and a step on the wheel's radius, which needs to be removed by dressing when the critical wear is reached. In angle-plunge grinding [11], the wheel is fed into the workpiece radially and axially simultaneously. The wheel moves radially, like in radial plunge grinding, but only for a small distance and at the same time, it moves parallel with the crankshaft rotational axis towards the side wall for a certain distance, see Fig. 6b.



**Fig. 6.** a) Radial plunge grinding and b) angular plunge grinding of the crankpin.

Oliveira et al. [10] compared axial and radial plunge strategies. Their research highlighted that the radial plunge grinding caused excessive wheel wear, while axial plunge grinding affected a very narrow portion of the wheel, causing wheel loading and workpiece burn. Consequently, researchers provided an alternative grinding of the crankpin by plunging axially at different radial steps, suggesting this strategy to reduce excessive heat generation on the sidewall and grinding wheel wear on the radius.

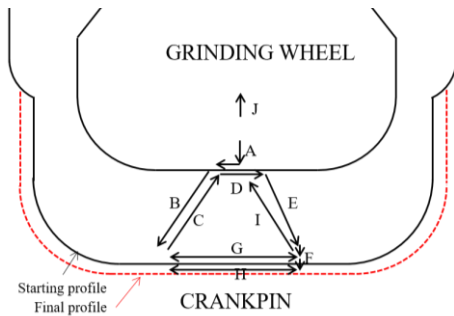
Comley et al. [3] utilised a high-efficiency deep grinding (HEDG) method using single-layer tools for grinding of crankpins. They have found this method particularly suitable for the rough grinding of sidewalls, offering improved productivity and reduced likelihood of thermal

damage. This phenomenon was explained by increasing heat removal via chip when increasing the material removal rate in HEDG regime.

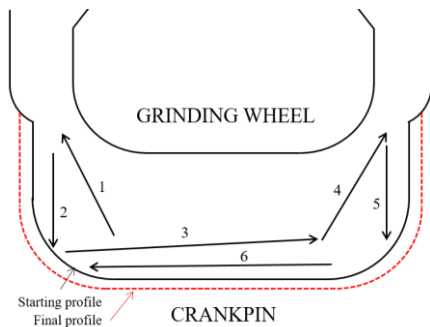
## 2.2 Crankpin grinding strategies developed by machine builders

Machine builders like Ervin Junker Maschinenfabrik, JTEKT Corporation and Fives Landis proposed different grinding strategies to improve crankpin grinding. Some of them have been built into their machine's NC control. A few methods are summarised in Tab. 1. More details can be found in Paper II.

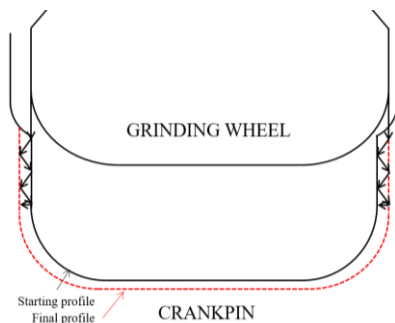
**Tab. 1.** Crankpin grinding strategies.



**Fig. 7.** Angle plunge grinding process developed by Toyota Koki Kabushiki Kaisha (JTEKT Corporation) to improve, at the time state-of-the-art, radial plunge grinding. The letters in the figure represent grinding steps [9].



**Fig. 8.** An alternative method proposed by JTEKT Corporation to avoid excessive wear on the radius. The numbers in the figure represent consecutive grinding steps [12].



**Fig. 9.** A grinding method proposed to improve cooling of the sidewalls enabled by wheel shuttling, as highlighted by arrows (submitted by JTEKT Corporation) [13].

### 2.2.1.1 Temperature controlled grinding of a crankpin

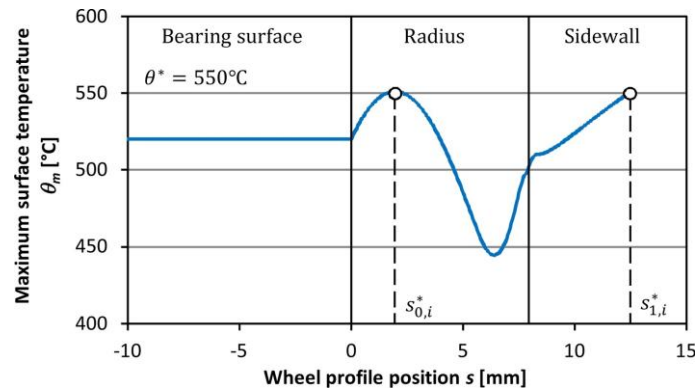
Recently, Drazumeric et al. [4] analytically modelled the crankpin grinding geometry and kinematics while incorporating a thermal model. This enabled to run the process at a set burn threshold, reducing the cycle time and hence improving the productivity.



A classical Jaeger's moving heat-source model [14] was used to calculate temperature at different portion of the wheel and define positions of the wheel that generate the most heat (Fig. 10). Then, each grinding increment (i.e., radial and axial feed per each workpiece revolution) was calculated in a way that the critical points on the wheel do not exceed a set maximum surface temperature, which can be calculated using the following formula:

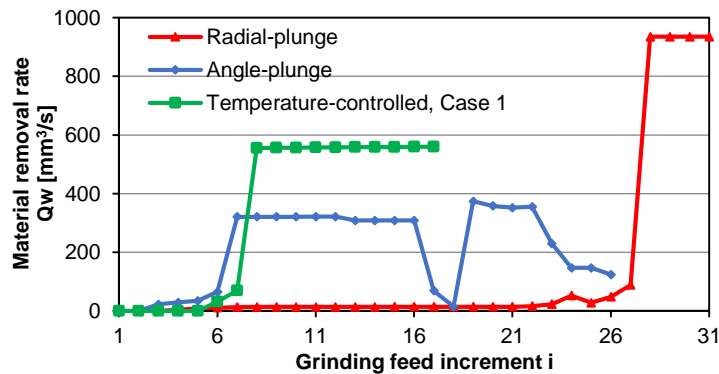
$$\theta^* = \frac{1.064}{\sqrt{k\rho c_p}} e_w [aggr(s, a_e^*)] \sqrt{\left(\frac{v_s}{10^6}\right) a_e^* aggr(s, a_e^*)} \rightarrow a_e^* = a_e^*(s, \theta^*) \quad (1)$$

where  $\theta^*$  is the pre-set critical maximum surface temperature,  $k$  is material thermal conductivity,  $\rho$  is density, and  $c_p$  is specific heat capacity of the workpiece material.  $a_e^*$  is the limit depth of cut calculated in every point of wheel profile,  $s$ ,  $v_s$  is the wheel speed,  $e_w$  is the specific grinding energy into the workpiece, which depends on aggressiveness and needs to be experimentally determined [2]. Aggressiveness ( $aggr(s, a_e^*)$ ) here is a non-dimensional parameter and is calculated for any position on the grinding wheel profile [15].



**Fig. 10.** Maximum surface temperature along the wheel profile (Reprinted from [2], with permission from Elsevier).

The productivity of three established strategies (radial vs. angular-plunge vs. temperature-controlled) was compared in production (see Fig. 11) [16]. The temperature-controlled method [17] significantly increased productivity by running a grinding process on a burn threshold – and removing the grinding allowance in less grinding feed increments.



**Fig. 11.** Comparison of cycle times for three different grinding strategies: radial- and angular-plunge, and temperature-controlled method (Adapted and modified from [16]).

### 2.3 Dressing strategies

The dressing is a crucial part of grinding, because it enables modification of the wheel surface to achieve a desirable grinding action. Dressing tool, dressing-system set-up, and dressing parameters affect grinding performance. While the first two are commonly defined by grinding tool manufacturers and machine builders, the grinding parameters can be modified by end users.

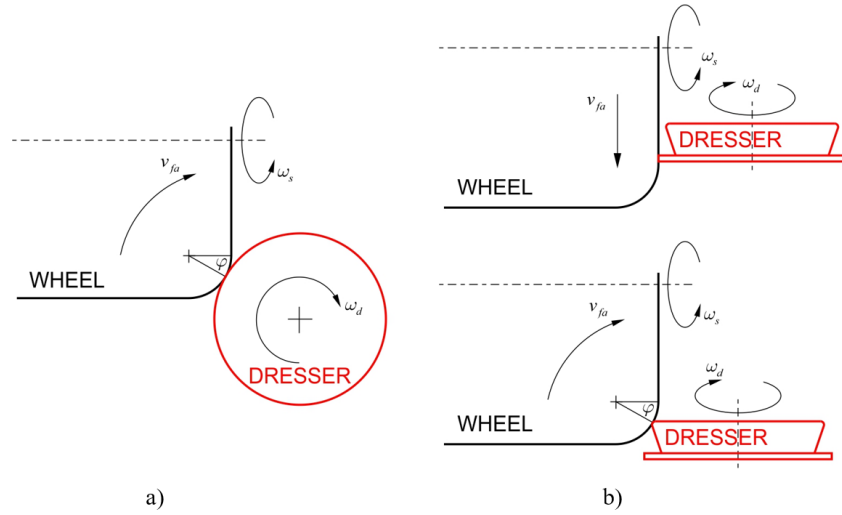
Over the years, a significant amount of research has been dedicated to the dressing process, particularly dressing parameters, as reviewed by Wegener et al. [18]. Different parameters have been used to explain the effect of dressing on grinding performance. Malkin and Murray [19] introduced an interference angle ( $\delta$ ) to indicate the severity of dressing. This parameter describes the relationship between in-feed speed ( $v_f$ ), dresser speed ( $v_d$ ) and grinding wheel speed ( $v_s$ ). Their research showed that a larger interference angle requires less dressing energy and has a higher probability of grit fracturing. On the other hand, a smaller interference angle results in grit flattening with higher dressing energy requirements. As investigated by Murray and Malkin [20], the interference angle also affects grinding performance. They observed that a larger interference angle reduces the grinding forces and increases workpiece surface roughness. The opposite trend was obtained with a smaller interference angle, i.e., with a dull-dressed wheel. Brinksmeier and Cinar [21] introduced the collision number ( $i_d$ ), which defines the number of collisions between the dresser diamond and the grinding wheel grits.  $i_d$  combines the dressing kinematics and the dressing/grinding wheel specifications but assumes the grit is spherical and the protrusion is constant. They noticed that a higher collision number results in grit flattening and higher grinding forces, and vice versa.

The dressing aggressiveness ( $Aggr_D$ ), recently introduced by Drazumeric et al. [4], is a more fundamental parameter to quantify the intensity of the abrasive interaction between the dresser and the grinding wheel. While the interference angle  $\delta$  is derived from a geometrical perspective, i.e. the angle at which a diamond attacks the grit in its trochoidal path in rotary dressing [19], the dressing aggressiveness  $Aggr_D$  is derived from the kinematics, i.e. the ratio of the normal to tangential component of the relative velocity vectors [4]. For rotary diamond dressing, this relationship becomes  $Aggr_D = 1/|1 - q_d|\sqrt{a_d/(d_e U_d)}$ , where  $a_d$  is the dresser infeed per wheel revolution,  $q_d$  is the dressing speed ratio (i.e. ratio between the rotary dresser speed and the grinding wheel speed), which has  $0 < q_d < 1$  values in uni-directional dressing and  $q_d < 0$  in anti-directional dressing;  $d_e$  is equivalent diameter; and  $U_d$  is the dressing overlap ratio.

Ishikawa and Kumar [22], Shaw [23] and Salje and Mackensen [24] discussed the importance of the overlap ratio ( $U_d$ ) during dressing.  $U_d$  defines the number of times the dressing tool touches a particular part of the grinding wheel surface. They observed more grit macro-fracture with lower  $U_d$ , and flatter grits and increased cutting point density with higher  $U_d$ . Another crucial parameter is the dressing speed ratio ( $q_d$ ), particularly relevant in rotary dressing processes. Spampinato and Axinte [25] confirmed a strong relation between  $q_d$ , dressing forces and wheel topography using numerical and experimental investigation.

Crankpin grinding requires dressing on the periphery (diameter), the radius and the sidewall portions of the wheel, making the dressing strategy more complex. Machine builders have

employed different dressing methods. Junker's crankshaft-grinders predominantly use two traverse dressers; a standard rotary dressing disc for the sidewall and the diamond cup wheel for the radius and the outer diameter of the cBN wheel (see Fig. 12b). The challenge of this method is that the dressing process is not continuous across the profile resulting in imperfections in geometry, particularly in transition between the side wall and the radius of the wheel. The second strategy is more common in Landis grinders (see Fig. 12a). They designed a cross-axial dressing which allows dressing of over  $180^\circ$  with a single geometry of the dressing roll. This provides more uniform dressing geometry around the different portions of the wheel.



**Fig. 12.** a) Cross-axial strategy allowing dressing across the whole wheel profile with a single geometry of a dressing roll and b) two-part dresser, where the cup wheel is used for the periphery (diameter) and the radius and the second dresser for the side wall [4].

## 2.4 Grinding wheel

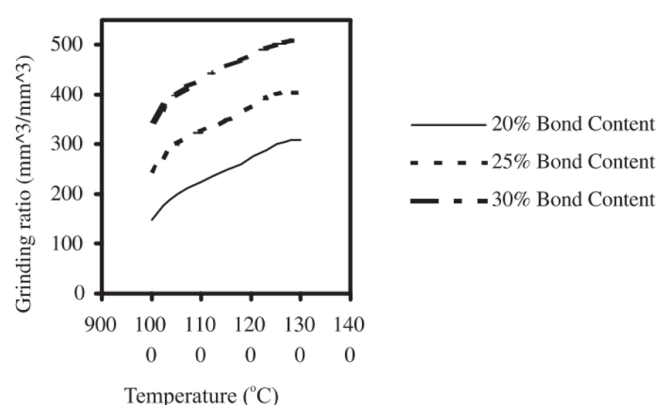
Grinding wheels can be broadly classified based on the abrasive they use (conventional or superabrasives) or the bond type (single layer, vitrified, resin or metal bonded). A vitrified bonded cBN wheel is the most commonly utilised tool in crankshaft grinding, particularly in high-volume automotive industry. In roughing operations, electroplated tools have proven to be very effective, achieving  $Q'$  of up to  $2000 \text{ mm}^3/\text{mm}\cdot\text{s}$  [3].

### 2.4.1 Vitrified bond system

Abrasive grits are held together with different bond materials. Most grinding wheels (conventional and superabrasive) feature vitrified bonds. The critical attribute of the vitrified bond is the sufficient bulk strength to primarily overcome stresses caused by the high peripheral speed of an operating wheel and to enable the adequate holding force of the cBN grits during the grinding process. Fluidity is another important parameter which indirectly describes the adhesion between the grit and the bond. The two properties can be altered by modifying the bond composition and sintering process. Yang et al. [26] extensively evaluated different bond components. They found that the overall bond strength increases when achieving the best match

in expansion coefficient between the cBN grains and the bond. Adding  $\text{TiO}_2$  material to the bond reduced fluidity, minimising the porosity and increasing the strength [27]. Similar results were achieved using  $\text{LiAlSi}_2\text{O}$  and  $\text{LiAlSi}_3\text{O}_8$  [28]. Wang et al. [29] used  $\text{ZrO}_2$  to reduce fluidity and improve the distribution of porosity, which increased the bond strength due to the improved adhesion of grit with the bond. However, while the bond has to have sufficient strength, it also has to be able to fracture, preferably in a controlled manner, to maintain the sharpness of the wheel for longer periods.

Jackson et al. [30] analyzed the interaction between the cBN surface and the bond. They observed a boric oxide layer that grows with increased sintering temperature. At the saturation point the thickness remains constant regardless of the temperature. As a result of boric oxide layer thickening, the tool life increases as shown in Fig. 13. Wheel life is expressed as G-ratio (G-ratio is defined as the volume ratio of workpiece material removed to wheel worn.) that increases with the higher percent of bond content and sintering temperatures.



**Fig. 13.** Grinding ration changes with sintering temperature (Reprinted from [30], with permission from Springer).

## 2.4.2 Porosity

Porosity has several important roles. Firstly, it gives the coolant the space to flow and transfers the heat from the grinding zone. Secondly, it provides the needed clearance for the grinding chips [31]. Considering it is an open, material-free space, it automatically reduces the friction and heat generation between the workpiece and the wheel (rubbing action). Carefully designed pores can also reduce crack propagation and, consequently, increase the impact strength of vitrified bonded tools [32].

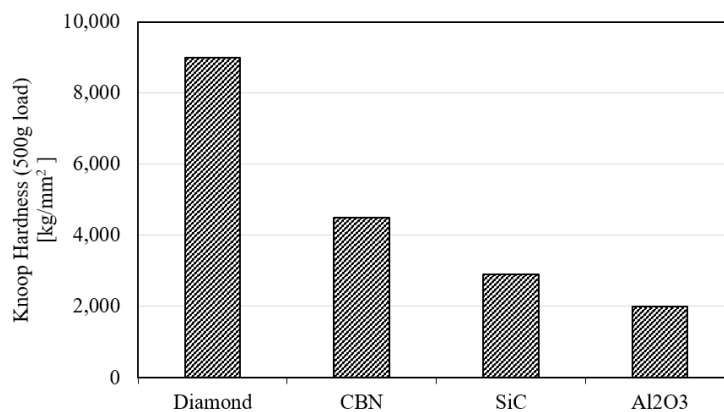
There are three main ways of introducing porosity into the vitrified bond wheel. The first, most straightforward way is to add pore former to the green body and let it burn off during sintering. This material is normally carbon-based, such as phenol resin and amorphous carbon [33]. Mao et al. [34] successfully used granulated sugar as a filler as it is readily available in different particle sizes and in large quantities. Similar results could also be obtained by using nut shells or PMMA (polymethylmethacrylate) microspheres [35]. The disadvantages of the aforementioned pore formers are that they can be challenging to remove and thus form defects on the product due to swelling. The second option was developed to reduce the challenges with conventional pore formers, where liquid  $\text{CO}_2$  is used as a solvent to remove pore inducers [36].

The third group of pore formers are ceramic materials designed as hollow shells, e.g. alumina bubble particles [37]. They form enclosed pores that fracture and open during the grinding process.

It is important to emphasise the importance of pores in vitrified bonded wheels. It is equally important to understand that poorly designed, e.g. too porous wheels, can lead to inadequate performance. For this reason, it is crucial to understand the requirements and challenges of the specific wheel application.

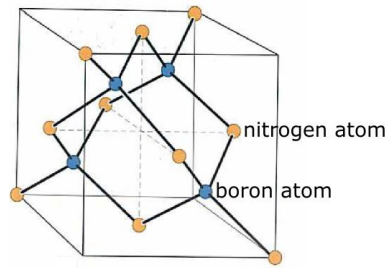
### 2.4.3 Cubic Boron Nitride (cBN) abrasive grit

There are two main abrasive families: (i) conventional and (ii) superabrasive. Superabrasives can be further divided into diamond and cBN. Nowadays, they are commonly used in the grinding industry due to their superior properties (see Fig. 14). cBN is particularly successful in ferrous grinding applications due to its chemical inertness and high thermal stability. Diamond, on the other hand, is a superior choice when grinding hard metals (e.g. tungsten carbide), ceramics, glasses and cermets, mainly due to its hardness. The downside of a diamond is that it deteriorates rapidly at elevated temperatures through graphitisation and oxidation [38], particularly in the presence of catalysts normally present in ferrous materials [39].



**Fig. 14.** Hardness differences of abrasives [40].

The first cBN synthesis was reported in 1956 [38]. However, the use in industrial grinding applications only started in the 1980s and early 1990s [41]. cBN is a transformation of hexagonal boron nitride to cubic boron nitride with the diamond lattice structure made up of boron and nitrogen atoms (Fig. 15). In his patent, Wentorf [38] described using boron or boron nitride in the presence of at least one catalyst to transform hBN to cBN at high pressures and high temperatures (HPHT).



**Fig. 15.** cBN lattice structure (Reprinted from [42], with permission from Element Six (UK) Ltd.).

Very little research was reported after the initial cBN development work. Only in the 1990s and 2000s did scientists become more interested in this topic. Different types of cBN grades also started emerging from grit manufacturers [43]. However, the synthesis and material properties were mostly kept as proprietary knowledge.

The key reason for changing the cBN manufacturing routes is to obtain different mechanical, geometrical or thermal properties to fit or improve the performance of the specific grinding operation. Grits properties can be altered by changing the raw input materials or modifying synthesis parameters. Both can be further divided into several subcategories, e.g., pressure, temperature, time, solvent choice, seeding, spontaneous nucleation, etc., generating numerous combinations. Nevertheless, each selection of raw material and/or synthesis parameters will generate its boundaries [44].

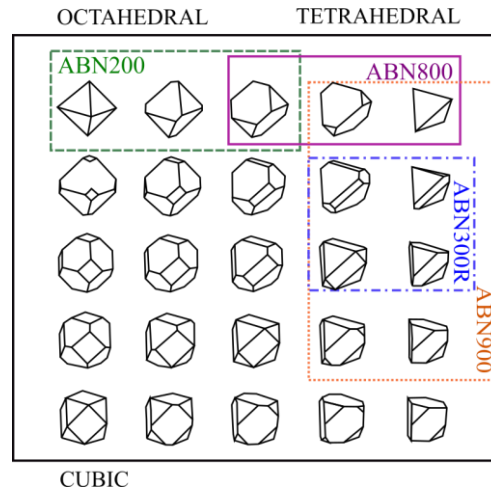
Taniguchi focused his research on synthesising high-purity large cBN grits to utilise electrical and optical properties. Together with Yamaoka [45], they reported a successful synthesis of large colourless (using barium boron nitride solvent) and amber crystals (using lithium boron nitride solvent) through spontaneous nucleation. They then doped cBN with Beryllium making dark blue cBN exhibiting semiconducting characteristics [46]. Kubota and Taniguchi [47] developed a cBN phase diagram using a metal alloy solvent, i.e. nickel molybdenum.

The majority of cBN grit development has been focused on producing monocrystalline grit, which is most widely available commercially. Only limited research has been focused on different types of polycrystalline materials: ultrafine polycrystalline cBN [48], aggregated cBN (AcBN) [49], and polycrystalline cBN (PcBN) [50,51]. Researchers claim that their main advantage is better self-sharpening and more controlled fracturing that prolongs the tool's life. However, only limited versions of polycrystalline grits are commercially available, because of their mechanical properties and price.

cBN is intrinsically colourless [42], but most commercially available materials are brown, amber/golden or black due to different impurities and defects introduced by solvents and additives. Amber materials (e.g. ABN900) are well known to be used in electroplated tools, and brown materials are believed to perform the best in vitrified bonded tools (e.g. ABN800). Black cBN types are often considered inferior materials used in resin bonds and lower-strength vitrified bond wheels. Colour can be measured using a spectrophotometer.

Shape and morphology are sometimes used in the same context, however, they explain different cBN attributes. Morphology focuses on the growth characteristics rather than just the physical

shape of crystals [52]. It is more complex for cBN than for diamond due to structural symmetry loss and fractured surfaces. The morphologies of E6 commercially available products are presented in Fig. 16.



**Fig. 16.** Morphologies of Element Six cBN grades (Adopted and modified with permission from Element Six, (UK), Ltd.).

Surface purity is not a frequently discussed parameter but is important, particularly from the wheel manufacturing perspective. Grits containing surface impurities can cause issues such as wheel bloating, resulting in wheel fracture. For this reason, most grit manufacturers employ vigorous cleaning procedures before shipping to customers. Inductively Coupled Plasma Optical Emission Spectroscopy (ICP-OES) can be used to evaluate impurities on the surface. This technique identifies the majority of elements relevant to grits, including amounts.

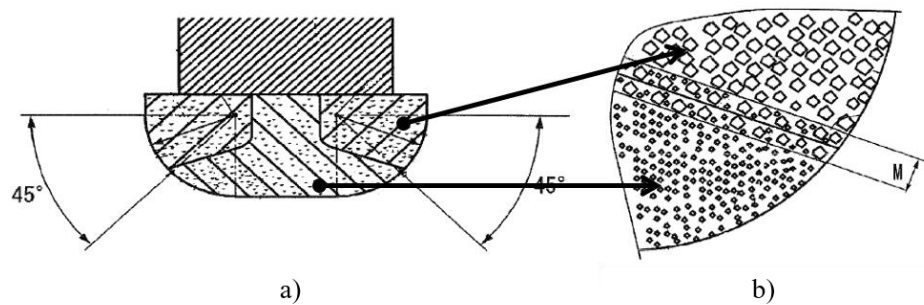
#### 2.4.4 State-of-the-art in crankpin grinding wheel designs

Grinding wheel wear was the primary driver of wheel developers to improve wheel designs. Achyutha and Radhakrishnan [53] conducted one of the earlier studies of grinding wheel wear in radial plunge grinding operation. They determined that wheel wear on the radius can only be removed by dressing, which reduces the wheel life. Thus, they proposed setting up a force threshold to help determine the dressing interval. In a subsequent paper, the same authors [6] focused on minimising the wear on the wheel's radius by grooving the grinding wheel on the side wall and radius. This led to reduced grinding forces and wheel wear due to minimised friction and improved cooling and cleaning capability.

There is a limited number of publications regarding grinding wheel designs to improve the grinding performance of crankpins. Although wheel makers likely keep it proprietary, some information can be obtained from their catalogues. Krebs and Riedel proposed a three-zone wheel for crankshaft grinding. They claim that the outside layers, covering the sidewalls and radii, are designed to maintain the profile [54]. The middle layer, covering the wheel's outer diameter, seems less critical. The majority of other wheel makers, Asahi Diamond Industrial Co.,Ltd., Saint Gobain Abrasives and Tyrolit - Schleifmittelwerke Swarovski AG & Co K.G,

to name a few, appear to have the same structure of the abrasive layer across the wheel profile. The composition usually contains one grit size (typically in the range of B151-B107) of high toughness and thermal stability grit in high concentration.

JTEKT Corporation [8] recently published a patent for a customised wheel (Fig. 17a) to overcome wheel-wear problems associated with the radial-plunge grinding of crankpins. The proposed design considers two different grit-bond systems (see Fig. 17b). The first section is designed with a hard bond system and coarser grits on the sidewall and a portion of the radius to increase wear resistance. The second zone on the lower part of the radius and the diameter of the wheel is composed of finer grit and a softer bond to generate a superior surface finish.



**Fig. 17.** a) Cross-section of the abrasive layer structure showing three distinctive sections where b) the sidewall and part of radius contain coarser grits and the rest of radius and diameter contain finer grits [8].



### 3 New crankpin grinding wheel development

The main objective of the thesis was to develop a new grinding wheel for the crankpin grinding process. The primary goals were to reduce heat on the sidewall and control wear at the upper sidewall interface. In this regard, it was essential to understand the grit wear mechanisms that commonly cause heat generation and excessive wheel wear.

Grinding processes mainly promote attritious (i.e. dulling of the tips of the abrasive grit) and fracture wear mechanisms. The attritious wear is caused by rubbing of the grits against the workpiece surface, which results in uniformly enlarged contact surface (wear flats), increasing heat generation and thermally damaging the workpiece [55]. Fracture wear is removal of grits from the wheel by grain fracture or bond fracture. This wear mechanism tends to change the general shape of the grit and is caused by a combination of thermal and mechanical stresses induced into the grit. Some level of fracture wear is desirable, keeping the grinding wheel sharp and allowing a free-cutting process with stable force. However, excessive grain and bond fracturing can shorten the wheel life. A mismatch between the grit and the bond can also cause grinding problems and severe wheel wear. Although less frequently, tough grit can break the bond during the process, not allowing the particles to work efficiently [56]. This phenomenon is caused by excessive dulling followed by wheel “collapse”, as observed by Badger [57].

Although considerable improvements have been observed in wheel design for crankshaft grinding, a fundamental investigation was required. First, it was essential to understand the critical grit properties that affect grinding wheel performance and wear. In addition, even though the approach proposed by JTEKT Corporation [8] with two layers was a plausible solution, the idea of using coarser grits on the side wall and finer grits on the radius and cylindrical bearing surface was questionable.

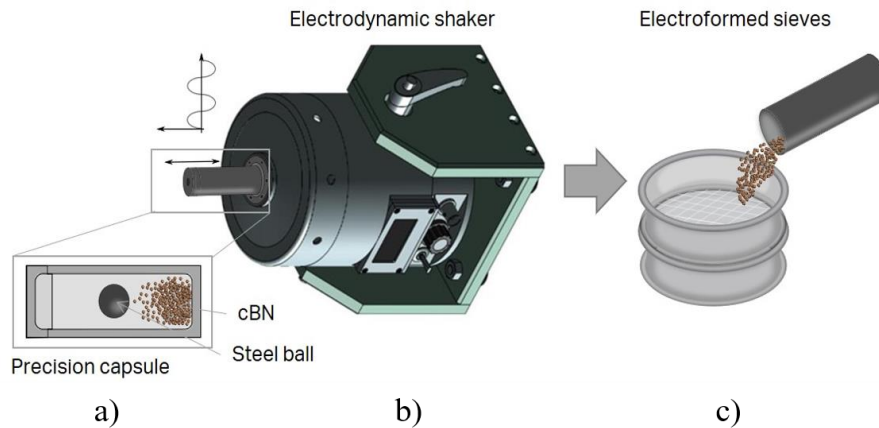
#### 3.1 Grit properties and characterisation

The effects of grit properties on grinding performance and wear were at the forefront of research presented in this thesis and the majority of the attached papers (Papers I, II, IV and V). This was possible by the fact that the grit manufacturer (E6) was the main project contributor, allowing grit customisation. Besides the grit characteristics mentioned previously, toughness ( $TI$ ), thermal stability ( $TS$ ) and aspect ratio ( $AR$ ) were the key grit properties evaluated in this work.

The  $TI$  measures a grit's resistance to fracture. It is an arbitrary measure of the breakdown resistance of the abrasive under impact loading. A high  $TI$  signifies a low percentage breakdown of grits. Thermal stability is the grit's ability to maintain its properties (hardness, toughness, resistance to oxidation and chemical breakdown, etc.) at elevated temperatures. Despite the availability of an international standard [58], grit manufacturers tend to develop their proprietary techniques for evaluating mechanical properties. The mentioned international standard quantifies the toughness by measuring the time at which approximately 50% of starting material is left on a defined sieve after an oscillatory motion of a precision capsule containing grit and a steel ball [58]. In all studies presented in this thesis, a steel ball and a specified amount

of grits were placed into a precision capsule, which was mounted to an electrodynamic shaker, and run for a set amount of time Fig. 18. Fractured material was then sieved, and grits left on the defined sieve were weighed and compared to the weight of the original material. Typically, tougher grits (higher  $TI$ ) retain more of the material in its original size range. Thermal stability was measured similarly after exposing the grit to elevated temperatures (1100°C), i.e. thermal stability defines toughness changes after high-temperature exposure. Indeed,  $TS$  is relevant for the wheel-making process [59], in which the temperatures can reach high enough levels, reducing the toughness of the grit.

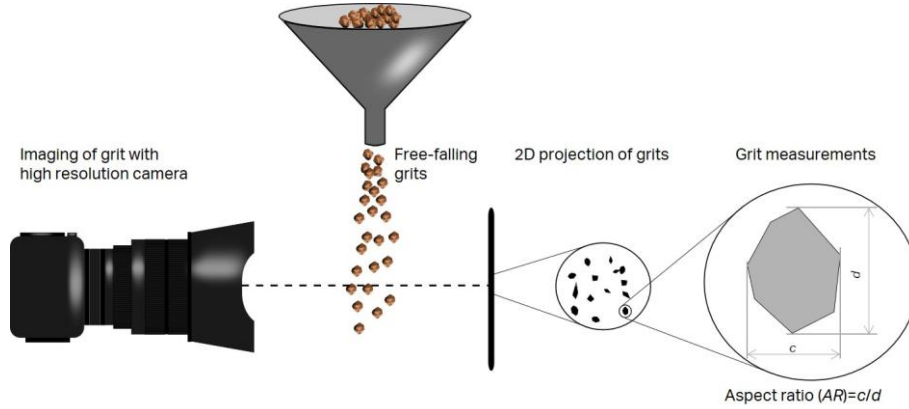
Both the  $TI$  and  $TS$  properties determine how well a grinding wheel can resist wear and, consequently, retain its surface topography. Broadly speaking, grits with higher values of  $TI$  and  $TS$  last longer, while weaker grits (lower values of  $TI$  and  $TS$ ) break down faster, resulting in a shorter tool life (lower G-ratio) [60]. Wheels with low values of  $TI$  and  $TS$  typically (but not always) require more frequent dressing. However, wheels containing grits with low  $TI$  can have the benefit of being “self-sharpening”, meaning dull grits fracture to expose new, sharp cutting edges.



**Fig. 18.** Friability test used to measure the toughness of grits and the thermal stability of grit that has been exposed to 1100°C. a) A precision capsule containing a grit sample and steel ball, b) an electrodynamic shaker and c) sieving of fractured material on the defined sieve [61].

The shape of the grit has become a crucial parameter, not only for grits in size range up to 50 $\mu\text{m}$  but also for coarser grits up to 250 $\mu\text{m}$ . Grit products with finer sizes are required to have a uniform shape to ensure a high-quality surface finish (e.g. wafers for semiconductors, finishing of crankshafts). In the coarser range, the shape has proven to modify the performance making it more free-cutting or improving the surface quality. The grinding community frequently uses adjectives to describe grit shape, e.g. elongated or blocky. There are measuring devices available that can evaluate grit shape. For example, Camsizer<sup>®</sup> XT device by Retsch Technology uses a dual camera system to capture larger and smaller grits. The challenge with most measuring techniques is the fact that they can only evaluate two-dimensional shapes. Chen et al. [62] recently introduced an alternative set of grit shapes based on 3D geometries. They claimed that each grit sample consists of a limited number of different geometries that should be considered when evaluating the grinding performance.

Although several different geometrical parameters are obtainable from commercial instruments, grits' average aspect ( $AR$ ) ratio is the most common shape factor used by grits manufacturers. According to international standards, grit size is determined through sieving [63,64] however can be determined with Camsizer<sup>®</sup> XT device through shortest cord measurement ( $c$ ) as highlighted in Fig. 19. Average aspect ratio ( $AR$ ), is captured from 2D-image projections as schematically shown in Fig. 19. The aspect ratio is defined as the ratio between the shortest cord and longest Feret diameter of grits in 2D projections.

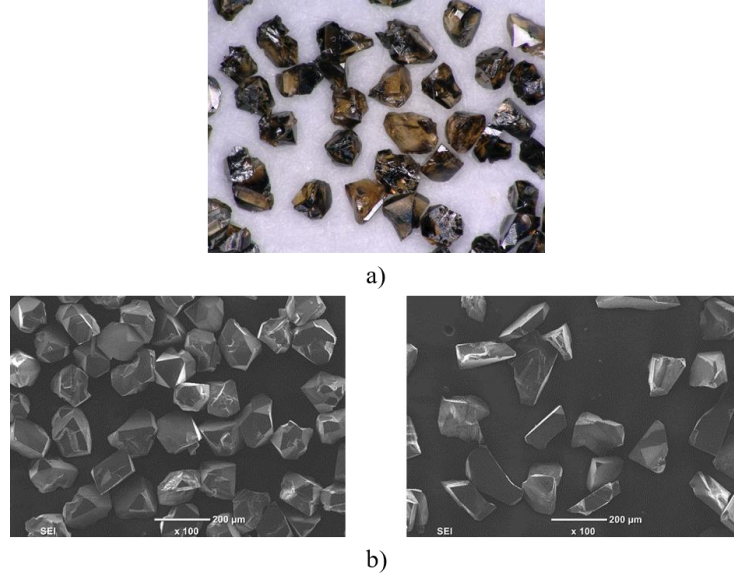


**Fig. 19.** Schematic illustration of average aspect ratio ( $AR$ ) estimation for grits (adapted from [65]).  $AR = c/d$  is based on the shortest chord  $c$  (generally equivalent to sieving) and the longest Feret diameter  $d$  obtained from a 2D projected image of a grit. The shortest cord  $c$  is also used to express the size of the grit [61].

Grits used in case studies presented in Chapter 3.4 are summarised in Tab. 2. Only the most relevant mechanical and geometrical properties were measured for a specific case study. A few selected grits are shown in Fig. 20.

**Tab. 2.** Evaluated properties of grit tested in grinding wheels in subsequent case studies.

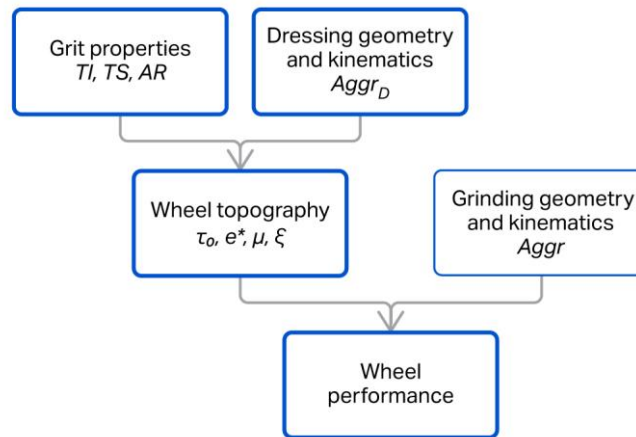
Grit type	$AR$	$TI$ (%)	$TS$ (%)	Grit size according to FEPA	Case study
Grit A	1.29	61.8		B126	Effects of grit shape
Grit B	1.39	66.1		B126	
Grit C	1.49	61.8		B126	
Grit D	1.5	60		B126	
Grit E	1.54	62.4		B126	
Grit F	1.85	56.8		B126	
ABN800		51.3	95	B151	Effects of grit concentration
ABN800		67.6	93	B181	Effects of grit size
ABN800		59.3	96	B126	
ABN800		71.1	98	B64	



**Fig. 20.** Different grit types used in the evaluation of grinding performance; a) ABN800 used in the evaluation of effects of grit size and concentration, b) blocky (left) and elongated (right) grits used in the evaluation of grit shape effects.

### 3.2 Analytical assessment framework for evaluation of grinding wheel performance

A novel analytical assessment framework was developed to better understand how grit properties affect wheel topography and grinding performance. Four new assessment parameters were proposed containing information regarding the topography of the grinding wheel (see Fig. 21). For more details, see Paper V.



**Fig. 21.** Wheel performance is affected by the grinding process (quantified via  $Aggr$ ) and wheel topography. It is measured by the newly introduced indicators  $\tau_0$ ,  $e^*$ ,  $\mu$ , and  $\xi$ . The wheel topography quantified with these indicators accounts for the synergistic effects between grit properties and dressing conditions (determined via  $Aggr_D$ ) [61].

The assessment framework was derived from Malkin and Cook's force model [55], where they divided the total force acting at the grit-workpiece interface into two independent components: (i) cutting (or shearing) ( $\mathbf{F}_c$ ), and (ii) rubbing and ploughing (which is often referred to simply as sliding) ( $\mathbf{F}_{sl}$ ):

$$\mathbf{F} = \mathbf{F}_c + \mathbf{F}_{sl} \quad (2)$$

$F_c$  is proportional to the cross-sectional cutting area that can be expressed as  $A_c = h_{eq}b$ . Therefore, the tangential and normal components of the cutting force can be written as:

$$F_c^t = e^* A_c \quad (3)$$

$$F_c^n = \frac{e^*}{\xi} A_c \quad (4)$$

where  $e^*$  ( $\text{J/mm}^3$ ) represents the intrinsic specific grinding energy, defined as the energy required to remove a unit volume of material for a given wheel topography and workpiece. The ratio  $\xi = F_c^t / F_c^n$  is the cutting-force ratio [2],  $h_{eq}$  is the equivalent chip thickness (defined by Snoeys and Peters in [66]), and  $b$  the width of grinding. It is important to note that the equivalent chip thickness does not account for the contact length  $l_c$ . Therefore, to fully incorporate the geometrical effect on the process, the aggressiveness number ( $Aggr$ ) is used as a fundamental, dimensionless parameter, where  $Aggr = h_{eq}/l_c$ . As a result,  $A_c$  can be expressed as  $A_c = Aggr \cdot l_c \cdot b$ .

The sliding components can be expressed as:

$$F_{sl}^t = \mu \bar{p} A_{sl} \quad (5)$$

$$F_{sl}^n = \bar{p} A_{sl} \quad (6)$$

where  $\mu$  is the friction coefficient at the grit-workpiece interface,  $\bar{p}$  is the average contact pressure between the wear flat and workpiece, and  $A_{sl}$  is the wheel wear flat area in  $\text{mm}^2$ , with  $A_{sl} = A l_c b$ , where  $A$  is the wheel wear-flat area, expressed as percentage. Based on experimental observations by Malkin and Cook [55],  $\mu$  and  $\bar{p}$  are assumed constant.

By combining Eq. 3, 4, 5 and 6, the following expressions can be derived:

$$F^t = (e^* Aggr + \mu \bar{p} A) l_c b \quad (7)$$

$$F^n = \left( \frac{e^*}{\xi} Aggr + \bar{p} A \right) l_c b \quad (8)$$

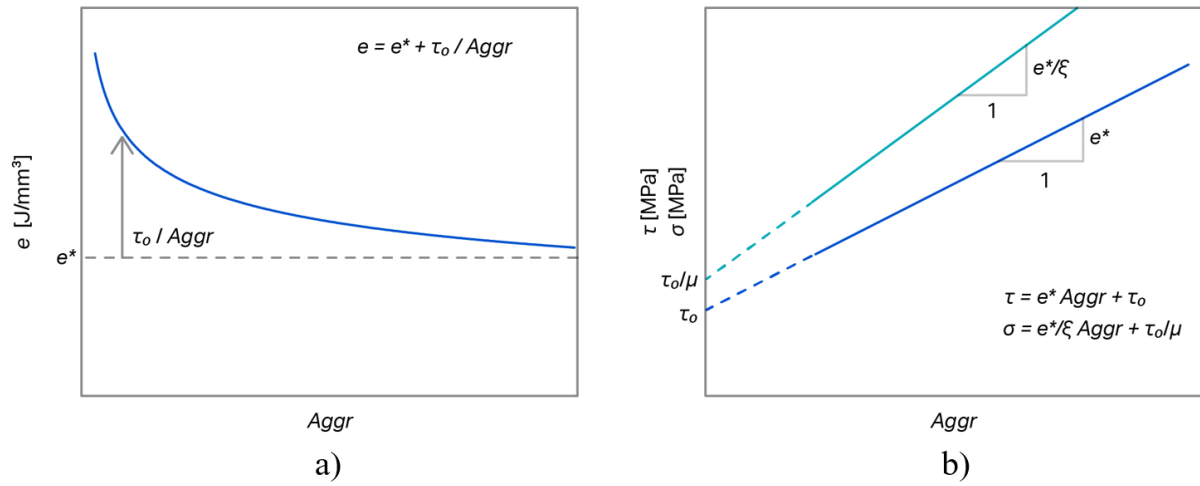
To generalise the assessment even further and to gain a fundamental insight into the mechanics of wheel-workpiece interface laws, the stress relationships are derived for the grinding contact by normalising the forces with  $l_c b$ , thus removing the geometrical and kinematical effects of the process and focusing only on evaluating the wheel topography and workpiece:

$$\tau = e^* Aggr + \tau_0 \quad (9)$$

$$\sigma = \frac{e^*}{\xi} Aggr + \frac{\tau_0}{\mu} \quad (10)$$

where  $\sigma = F^n / l_c b$  is the normal stress,  $\tau = F^t / l_c b$  is the tangential stress, and  $\tau_0 = \mu \bar{p} A$  is the sliding component of the tangential stress. The above stress variables have the units MPa, while the intrinsic specific grinding energy has the units  $\text{J/mm}^3$ .

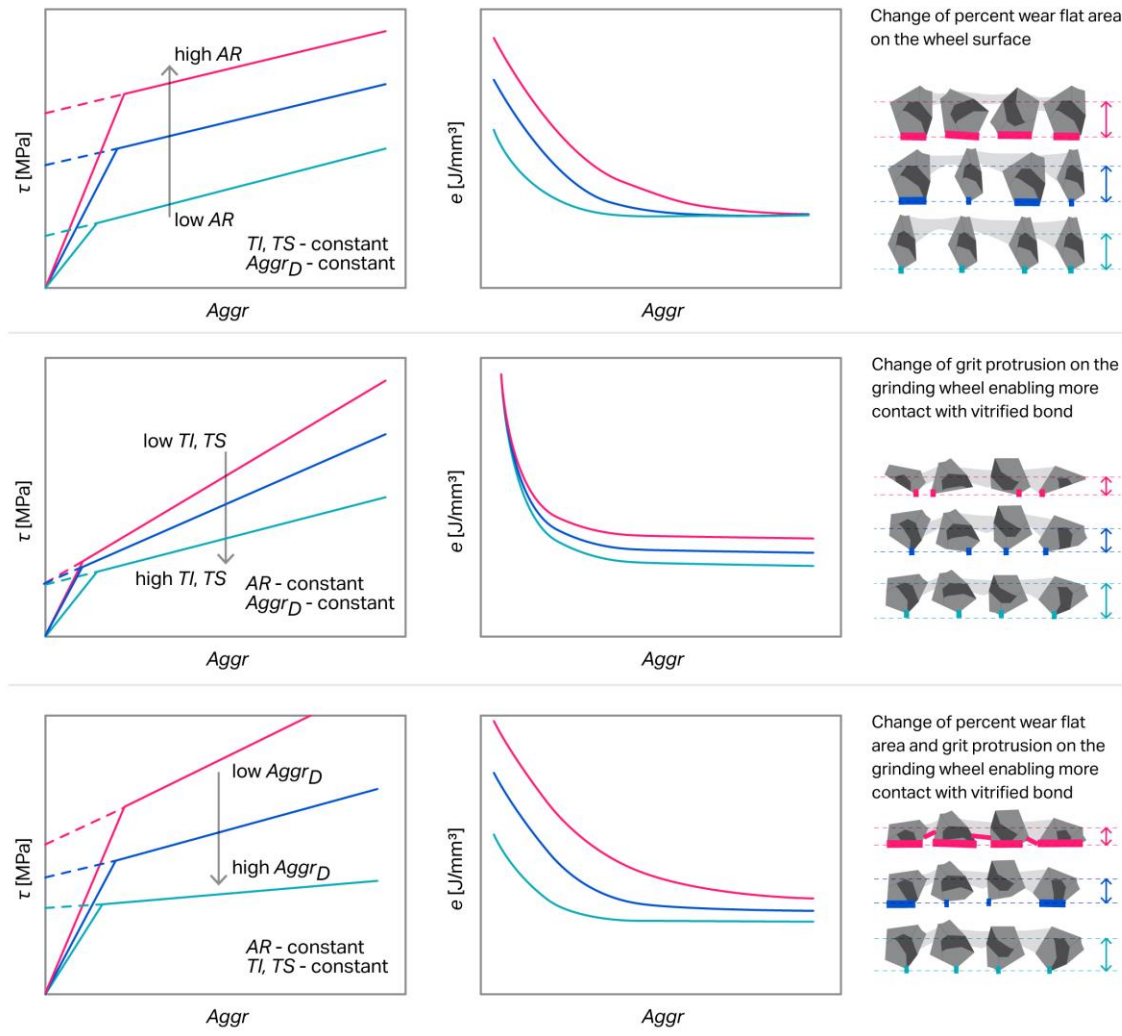
A schematic illustration of grinding-response assessments is shown in Fig. 22a. While the characteristic total specific energy curve is the most common indicator of grinding efficiency for a given wheel-workpiece combination and a given set of dressing and cooling conditions, it does not directly link with wheel topography. In addition, it is challenging to distinguish between the energy associated with cutting and the energy associated with sliding. On the other hand, the proposed performance assessment (Fig. 22b) is capable of quantifying and evaluating the topography effects via the four performance indicators:  $e^*$ ,  $\tau_0$ ,  $\mu$  and  $\xi$ . The parameter  $e^*$  can be extracted from the slope of the  $Aggr - \tau$  curve, and the parameter  $\tau_0$  can be extracted from the intercept. Considering also the normal stress  $\sigma$ , additional parameters  $\xi$  and  $\mu$  can be obtained. The latter,  $\mu$ , is a ratio of the intercepts of the linear regression applied to the pairs  $(Aggr, \tau)$  and  $(Aggr, \sigma)$ . The proposed parameters ( $e^*$ ,  $\tau_0$ ,  $\xi$  and  $\mu$ ) are hence useful quantitative indicators of the wheel performance over a range of grinding conditions for an arbitrary  $Aggr$ , i.e. a given grinding process geometry and kinematics.



**Fig. 22.** Wheel-performance indicators vs grinding aggressiveness. The graphs are plotted as: a) the characteristic specific energy curve [4]; and b) the grinding response in  $(Aggr, \tau)$  and  $(Aggr, \sigma)$  diagrams, where the introduced performance indicators can be easily obtained ( $e^*$ ,  $\tau_0$ ,  $\xi$  and  $\mu$ ). Note that the illustrations are general, i.e., not based on actual measurements [61].

Note that all proposed variables are normalised. From a practical point of view, introducing the scaled variables removes the influence of the wheel width and contact length. Hence, the grinding responses of different wheels and depths of cut can be fundamentally analysed and compared.

Case studies presented in Paper V enabled to generalise the findings with regard to grinding responses based on grit properties ( $TI$  and  $TS$ ) and dressing conditions ( $Aggr_D$ ), as shown in Fig. 23. The characteristic grinding responses are schematically illustrated in the  $Aggr - \tau$  and  $Aggr - e$  plots. Additionally, the characteristics of the wheel topography are exemplified for different values of percent wear-flat area  $A$  and grit protrusion  $\Delta\alpha$ .



**Fig. 23.** A conceptual depiction of grinding response and wheel performance for different grit properties ( $TI$ ,  $TS$ ,  $AR$ ) and dressing conditions ( $Aggr_D$ ). This framework can be utilised to foresee the theoretical performance changes of various grinding wheels dressed in different ways. The left column shows tangential stress vs aggressiveness, the middle column shows specific energy vs. aggressiveness, and the right column illustrates the wheel-workpiece interface in terms of percent of wear flat area  $A$  and grit protrusion  $\Delta\alpha$  [61].

### 3.3 Laboratory tests to evaluate grit performance

Grinding tests, although lengthy, are the most reliable method for direct evaluation of wheel performance. Two rigorous types of experiments were carried out in the laboratory environment to assess the performance of grits: (i) window-of-operation test and (ii) wear test.

Grinding tests can be time-consuming and costly. Therefore, a novel lapping-based method was also developed to evaluate the wear rate of cBN abrasive segments. Its primary benefits are short testing times and smaller specimen sizes. In addition, lapping-based tests can be primarily used for screening purposes for grit- and abrasive-tool manufacturers wishing to reduce time-consuming grinding experiments. The lapping-based method was the focus of Paper IV.



### 3.3.1 Grinding tests

All grinding tests were carried out using a Blohm MT408 surface grinding machine (see Fig. 24). The workpiece material was 100Cr6 (AISI/SAE 52100) a through-hardened bearing steel with a hardness of 60-61HRC. Forces were measured with a two-component Kistler 9257A dynamometer. The grinding fluid was Hocut 768 water-based emulsion (4.5–5.0% concentration) delivered to the grinding zone at 9 bars. A 40-bar high-pressure cleaning nozzle was used to remove residue (loading) from the grinding-wheel pores.



**Fig. 24.** Blohm MT408 surface grinder [67].

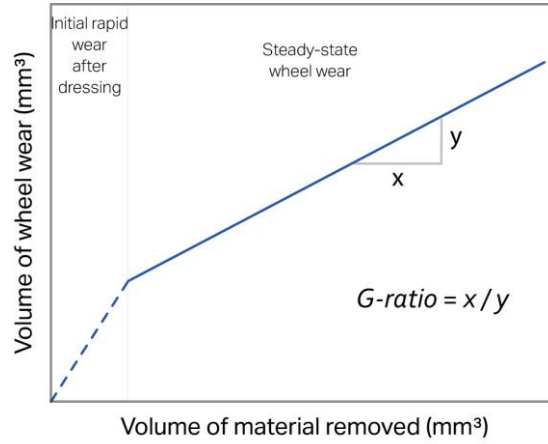
#### 3.3.1.1 Window of operation test (minimum wheel wear)

The window of operation test consisted of an initial dressing process followed by several (no-dress) grinding passes to stabilise the grinding force and eliminate the dressing effect (wheel break-in) [68]. Once the process was stabilised, various values of *Aggr* were imposed by changing workpiece speed, depth of cut and wheel speed. The number of passes per each *Aggr* was minimised to avoid grinding wheel wear, i.e., for a given workpiece and wheel topography, the wear flat area ( $A_{sl}$ ) is assumed constant. This is because cBN wheels wear significantly slower than conventional-abrasive wheels [69]. Thus, all variables of the assessment framework ( $e^*$ ,  $\tau_0$ ,  $\xi$ ,  $\mu$ ) could be estimated as shown in Fig. 22b. Indeed, the window of operation test provides the characteristic wheel-workpiece signature for a given machine and cooling/lubrication conditions.

#### 3.3.1.2 Wear test

The grindability can be evaluated via grinding wheel wear at a specific *Aggr* and dressing conditions (Fig. 25). The wear test consisted of a set workpiece volume ground utilising only half of the grinding wheel. The groove generated on the grinding wheel was used to measure the wheel wear (also known as a razor-blade technique). The wear in a shape of a step was measured using an optical 3D surface measurement system (Alicona G5). Surface roughness was also evaluated using a tactile surface-roughness tester (Taylor Hobson Surtronic S-100).

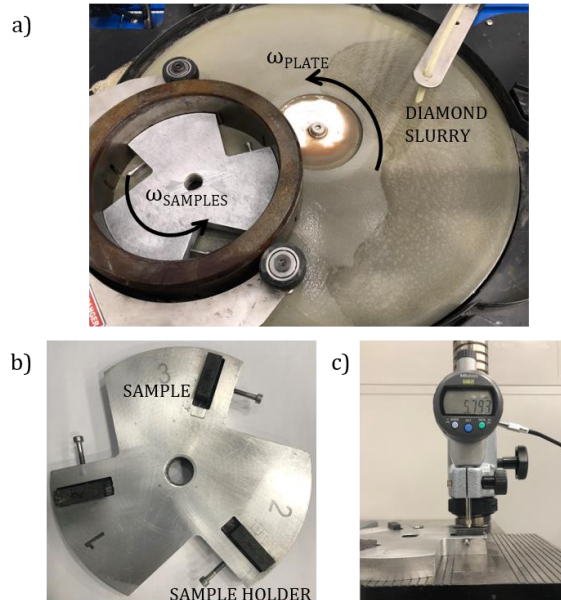




**Fig. 25.** A schematic illustration of grinding wheel wear progression.

### 3.3.2 A lapping-based test method

A novel lapping-based method is proposed for evaluation of grit-bond systems used in grinding wheels. Its primary benefits are short testing times and smaller specimen sizes. A lapping-based test method was developed and implemented using a Lapmaster Wolters Model 15 lapping machine (Fig. 26a) equipped with a speed controller and a timer. The lapping plate (diameter 304.8 mm) was made of solid cast iron. The cBN segments were mounted onto a customised jig (Fig. 26b). Three 120°-spaced segments (width = 8 mm, height = 10.5 mm, length = 25 mm) were lapped simultaneously.

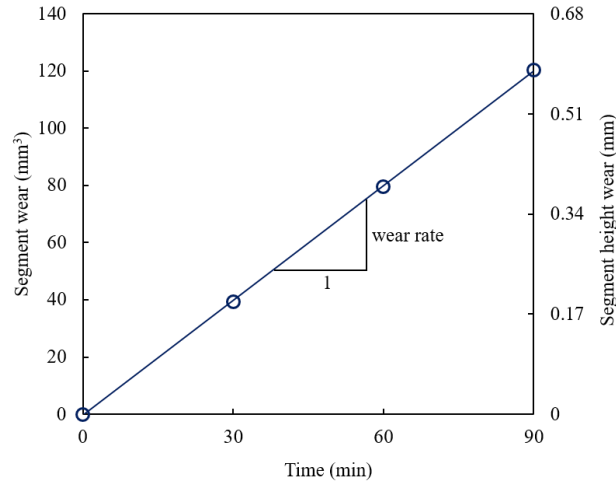


**Fig. 26.** a) Lapping set-up, b) jig holding the cBN segments, and c) measurements of segment height during the test [70].

The slurry used to accelerate the wear of the segments consisted of a diamond-suspension liquid containing 20- $\mu$ m-diameter (on average) diamond abrasive in 150 ct/L concentration. The segments were conditioned for 60 minutes to flatten the samples using the same parameters as

the lapping tests, with a rotational lapping speed of 72 RPM. The slurry was added at 1 drop/second. The sample load was created by the jig's weight (0.5 kg).

After the conditioning, the segments were lapped for three, 30-minute intervals. The height of the sample was measured at the beginning of the test and at the end of each interval using an electronic depth gauge (Fig. 26c) with a resolution of 0.1  $\mu\text{m}$ . The wear rate was calculated in  $\text{mm}^3/\text{min}$  using linear regression (see example in Fig. 27).



**Fig. 27.** Example of wear-rate measurements [70].

### 3.4 Results and discussion

#### 3.4.1 Grit shape (aspect ratio- $AR$ ) effects on grinding performance

Six monocrystalline grits, Grit A – Grit F (see Tab. 2), with an average size 126 $\mu\text{m}$  (FEPA B126 or ANSI 120140), were made into grinding wheels with the same composition (concentration, bond quality and amount of porosity) and tested in grinding trials as summarised in Paper III. The grit concentration in wheels is comparable to the one in crankshaft grinding wheels ( $C=150 \rightarrow 6.6 \text{ ct}/\text{cm}^3$ ).

The dressing and grinding parameters used in trials are summarised in Tab. 3 and Tab. 4 respectively. The grinding parameters were chosen to match the aggressiveness of the industrial crankshaft grinding process, particularly on the bearing surface.

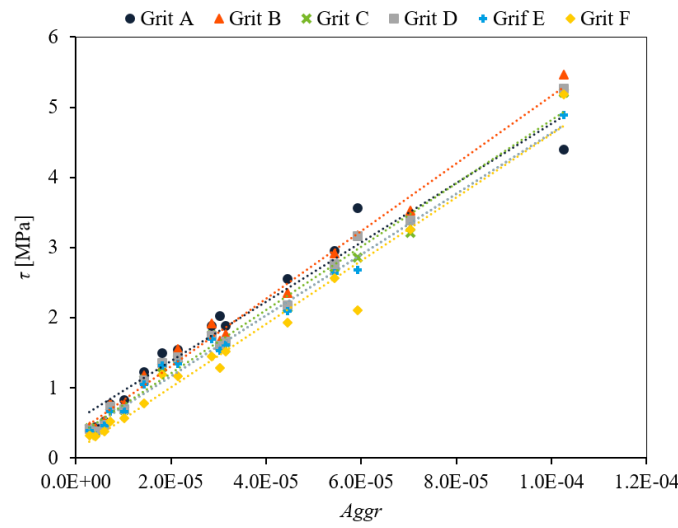
**Tab. 3.** Dressing parameters.

<b>Overlap ratio, <math>U_d</math></b>	4
<b>Dressing depth, <math>a_d</math></b>	0.003 mm
<b>Dressing speed ratio, <math>q_d</math></b>	0.81

**Tab. 4.** Grinding parameters for a window of operation test.

<b>Wheel speed, <math>v_s</math></b>	40 m/s
<b>Depth of cut, <math>a_e</math></b>	0.01 - 0.3 mm
<b>Workpiece speed, <math>v_w</math></b>	1.2 - 24.6 m/min
<b>Specific material removal rate, <math>Q'</math></b>	0.6 - 33 mm <sup>3</sup> /mm·s
<b>Aggressiveness, <math>Aggr</math></b>	$2.86 \cdot 10^{-6} - 1.03 \cdot 10^{-4}$

The results of the window of operation trials are shown in Fig. 28. Considering also  $Aggr - \sigma$ , four performance indicators for all six grit types were extracted. They are summarized in Tab. 5.

**Fig. 28.** Window of operation results for grit with different aspect ratios but comparable toughness.**Tab. 5.** Performance indicators ( $e^*$ ,  $\tau_0$ ,  $\xi$  and  $\mu$ ) for six grit types with different AR.

Grit type	AR	$e^*$ (J/mm <sup>3</sup> )	$\tau_0$ (MPa)	$\xi$	$\mu$
Grit A	1.29	49	0.53	0.36	0.15
Grit B	1.39	49	0.33	0.38	0.13
Grit C	1.49	46	0.30	0.38	0.16
Grit D	1.5	48	0.29	0.36	0.12
Grit E	1.54	45	0.29	0.37	0.13
Grit F	1.85	46	0.11	0.43	0.12

The general understanding in the grinding research is that grit shape affects the grinding efficiency, and with this the related  $e^*$ . This is based on the evaluation of the total specific grinding energy curve where it is challenging to distinguish between the energy associated with cutting ( $e^*$ ) and the energy associated with rubbing and ploughing ( $\tau_0/Aggr$ )- see Fig. 22a.

Results in Fig. 28, however, show that the inclination of the trend lines is similar for all tested grits, which is reflected in the intrinsic specific grinding energy  $e^*$  (see Tab. 5). This suggests that grit shape does not affect the grinding efficiency ( $e^*$ ).

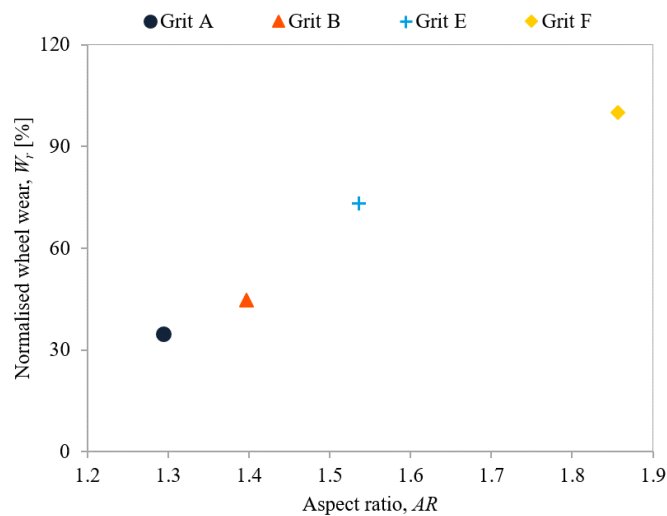
The sliding component of tangential stress ( $\tau_0$ ) on the other hand, varies with the grits'  $AR$ . The grit with lower  $AR$  (blocky) generates higher values of  $\tau_0$  and vice versa. In Paper V these two parameters were correlated to grits' protrusion and percent wear flat area ( $A$ ) on the wheel surface, respectively. This was examined through optical microscopy of the grinding wheel surface, which was correlated with grinding performance indicators. By applying the same principle, it can be concluded that protrusion of grits does not vary significantly with  $AR$ , however, the percent wear flat area ( $A$ ) does. The cutting force ratio ( $\xi$ ) is comparable for the grits regardless of the shape. The same is observed for  $\mu$ , which is generally low and comparable to the one between diamond and metal [71].

Wear tests were carried out at a constant  $Aggr$  (see Tab. 6) after dressing using parameters summarised in Tab. 3. Four grit types were tested in extended trials: Grit A, B, E and F.

**Tab. 6.** Grinding parameters for the wear test.

<b>Wheel speed, <math>v_s</math></b>	40 m/s
<b>Depth of cut, <math>a_e</math></b>	0.033 mm
<b>Workpiece speed, <math>v_w</math></b>	24 m/min
<b>Specific material removal rate, <math>Q'</math></b>	13.2 mm <sup>3</sup> /mm·s
<b>Aggressiveness, <math>Aggr</math></b>	1.05·10 <sup>-4</sup>
<b>Total volume ground</b>	7.6 cm <sup>3</sup> /mm

The grinding wheel wear is shown in Fig. 29. The results were normalised with respect to the highest value. The general trend is that grits with lower  $AR$  (blocky) generate higher forces and, consequently, lower grinding wheel wear.



**Fig. 29.** Correlation between the wheel wear and the aspect ratio of grit.

### 3.4.2 Grit concentration effects on grinding performance

The concentration of the grinding wheel is defined by the amount of cBN grits in a specific volume, i.e. concentration 100 is equal to 4.4 carats of cBN grit in  $1\text{cm}^3$  of the wheel. High concentration grinding wheels are standard in applications where the contact between the grinding wheel and the workpiece is relatively low, e.g. crankpin bearing grinding. A higher number of effective grains can cause more rubbing and heat leading to thermal damage. Keeping the contact length ( $l_c$ ) low, this likelihood can be minimised, and the benefits of extended tool life can emerge.

Two grinding wheels with different grit concentrations were tested. Both had equal amounts of porosity and bond but variable quantities of cBN. Secondary abrasives were used to substitute the missing cBN in the lower concentration wheel. Grit was ABN800 B151 that came from the same batch and thus had the same properties, i.e. the same  $TI$ ,  $TS$  and  $AR$  (see Tab. 2). Dressing and grinding parameters for a window of operation test are summarised in Tab. 7 and Tab. 8.

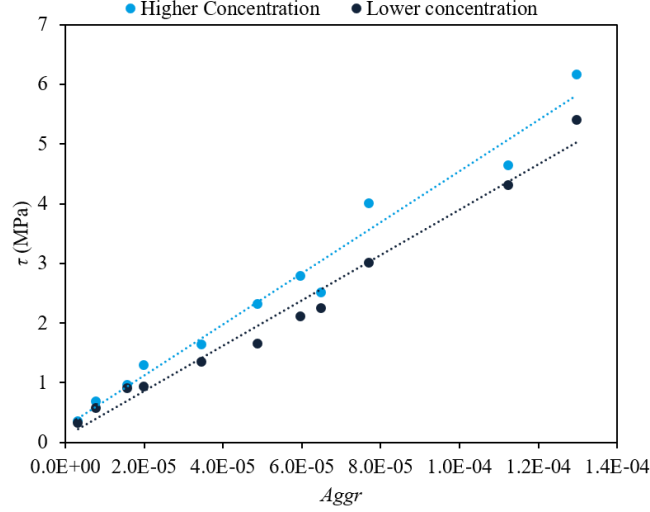
**Tab. 7.** Dressing parameters.

<b>Overlap ratio, <math>U_d</math></b>	4
<b>Dressing depth, <math>a_d</math></b>	0.003 mm
<b>Dressing speed ratio, <math>q_d</math></b>	0.81

**Tab. 8.** Grinding parameters for a window of operation test.

<b>Wheel speed, <math>v_s</math></b>	40 m/s
<b>Depth of cut, <math>a_e</math></b>	0.01 - 0.3 mm
<b>Workpiece speed, <math>v_w</math></b>	1.2 - 24.6 m/min
<b>Specific material removal rate, <math>Q'</math></b>	0.6 - 33 $\text{mm}^3/\text{mm}\cdot\text{s}$
<b>Aggressiveness, <math>Aggr</math></b>	$3.1\cdot 10^{-6} - 1.3\cdot 10^{-4}$

The results of the window of operation tests are displayed in Fig. 30. Considering also  $Aggr - \sigma$ , four performance indicators for two different grit concentrations were extracted. They are summarised in Tab. 9.



**Fig. 30.** Window of operation results for two wheels with different grit concentrations.

**Tab. 9.** Performance indicators ( $e^*$ ,  $\tau_0$ ,  $\xi$  and  $\mu$ ) for wheels with two different concentrations.

Grit type	Concentration	$e^*$ (J/mm <sup>3</sup> )	$\tau_0$ (MPa)	$\xi$	$\mu$
ABN800	Higher	43.1	0.26	0.45	0.12
ABN800	Lower	37.2	0.10	0.40	0.05

A 15% difference in intrinsic specific grinding energy ( $e^*$ ) can be observed, suggesting that a wheel with higher concentration is less efficient (in terms of cutting). Using the correlations between performance indicators and wheel topography, reported in Paper V, it can be concluded that grit protrusion is lower for a higher concentration wheel. Similarly, a sliding component of tangential stress ( $\tau_0$ ) is higher for a wheel with higher concentration, suggesting that more cBN particles per unit area cause an increase in the percent wear flat area ( $A$ )- see Tab. 9.

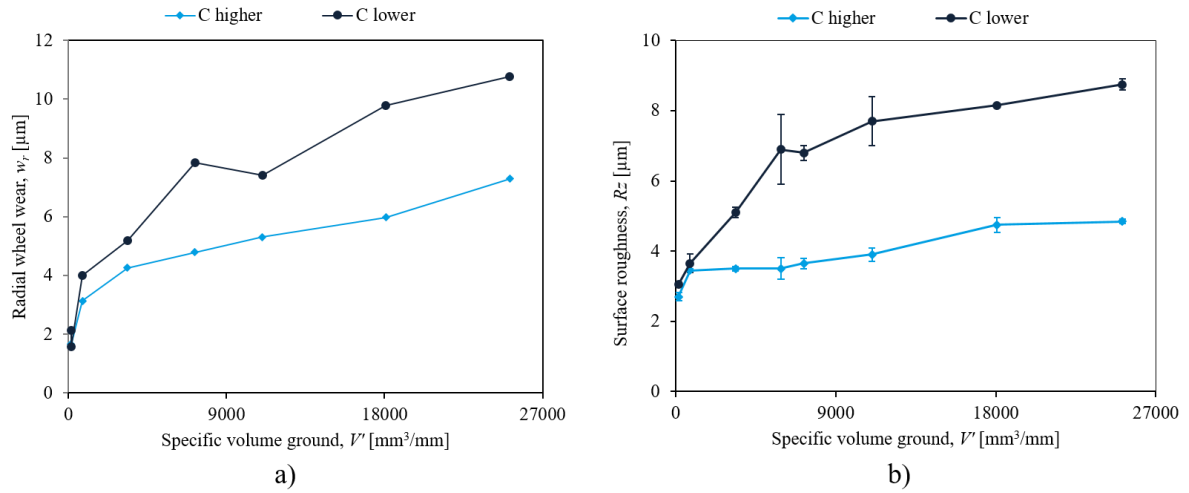
The grinding force ratio ( $\xi$ ) is similar for both wheels, however there is difference in friction coefficient ( $\mu$ ). Even though the  $\mu$  is in the same range for diamond-metal, the result could be suggesting additional rubbing when using a higher concentration wheel, which could be attributed to grit-bond contact.

Grinding parameters used for evaluation of the wheel wear are summarized in Tab. 10. The dressing parameters were the same as in the window of operation test (see Tab. 7). Low depth of cut was applied to ensure low  $l_c$ , common for high concentration grinding wheels.

**Tab. 10.** Grinding parameters for the wear test.

<b>Wheel speed, <math>v_s</math></b>	70 m/s
<b>Depth of cut, <math>a_e</math></b>	0.04 mm
<b>Workpiece speed, <math>v_w</math></b>	25 m/min
<b>Specific material removal rate, <math>Q'</math></b>	16.7 mm <sup>3</sup> /mm·s
<b>Aggressiveness, <math>Aggr</math></b>	7.53·10 <sup>-5</sup>
<b>Total volume removed,</b>	25 cm <sup>3</sup> /mm

Wheel wear and workpiece surface roughness are shown in Fig. 31. Despite removing a high amount of material, only a few microns of wear were achieved. The levels are comparable to those achieved in real applications [72]. The results highlight that the lower concentration wheel wears faster (Fig. 31a) and produces higher surface roughness on the workpiece (Fig. 31b). The higher concentration cBN wheel results in lower force and improved surface finish.

**Fig. 31.** a) Grinding wheel wear and b) surface roughness generated during wear test.

### 3.4.3 Evaluation of effects of grit size

ABN800 with three different grit sizes, FEPA B181, B126 and B64 (see Tab. 2), were produced, and wheels with the same bond type manufactured and the concentration C125 (5.5 ct/cm<sup>3</sup>). By keeping the concentration constant, a higher number of grits per unit area in the wheel (i.e. cutting point density) is expected with smaller grit and vice versa. Dressing and grinding parameters are summarized in Tab. 11 and Tab. 12, respectively.

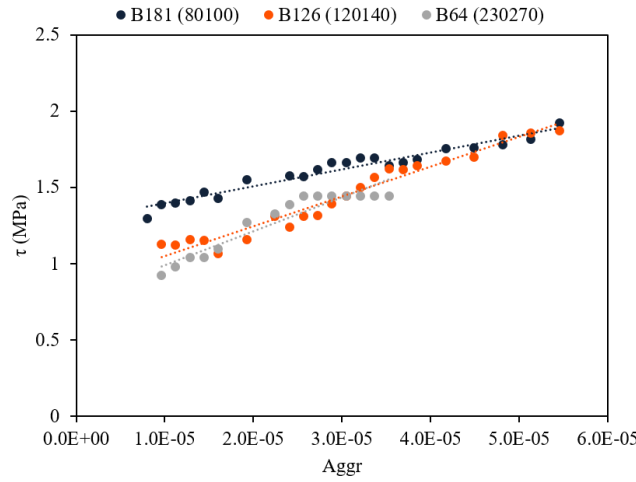
**Tab. 11.** Dressing parameters.

<b>Overlap ratio, <math>U_d</math></b>	4
<b>Dressing depth, <math>a_d</math></b>	0.003 mm
<b>Dressing speed ratio, <math>q_d</math></b>	0.81

**Tab. 12.** Grinding parameters for a window of operation test.

<b>Wheel speed, <math>v_s</math></b>	60 m/s
<b>Depth of cut, <math>a_e</math></b>	1 mm
<b>Workpiece speed, <math>v_w</math></b>	0.3 – 3.4 m/min
<b>Specific material removal rate, <math>Q'</math></b>	5 – 56.7 mm <sup>3</sup> /mm·s
<b>Aggressiveness, <math>Aggr</math></b>	$8.01 \cdot 10^{-6} - 5.45 \cdot 10^{-5}$

Window of operation results are shown in Fig. 32. Considering also  $Aggr - \sigma$ , four performance indicators for the three grit sizes were extracted. They are summarized in Tab. 13.

**Fig. 32.** Window of operation results for two wheels with different grit sizes.**Tab. 13.** Performance indicators ( $e^*$ ,  $\tau_0$ ,  $\xi$  and  $\mu$ ) for wheels with three different grit sizes.

Grit type	Grit size	$e^*$ (J/mm <sup>3</sup> )	$\tau_0$ (MPa)	$\xi$	$\mu$
ABN800	B181	11.1	1.28	0.51	0.28
ABN800	B126	19.4	0.85	0.62	0.22
ABN800	B64	22.2	0.77	0.61	0.26

Initially, it can be noticed that intrinsic specific grinding energy ( $e^*$ ) is significantly lower compared to previous case studies. This could be attributed to high grinding wheel porosity, lower grit concentration and the grinding parameters employed. Secondly, there is a considerable difference between wheels B181 and B64 regarding  $e^*$ . Correlating this to wheel topography, it can be concluded that the wheel containing smaller grits has a lower protrusion and, consequently higher  $e^*$ . Hence, the grinding process with smaller grit is less efficient than the one using coarser grits. Interestingly, a sliding component of tangential stress ( $\tau_0$ ), obtained from the intersection of the linear regression trend, is larger for coarser grit, i.e. the percent wear flat area ( $A$ ) is higher for coarser grit. In this case, larger grit sizes can naturally generate



a larger contact area, or the dressing process causes greater wear flats in large grits, as previously reported by Badger et al. [73].

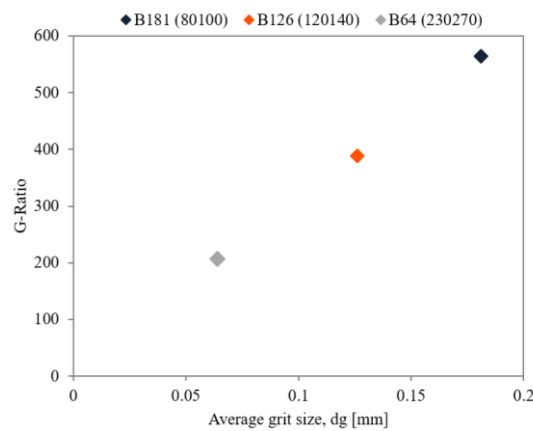
The grinding force ratio ( $\xi$ ) and friction coefficient ( $\mu$ ) are comparable for the three wheels.  $\mu$  is higher compared to wheels tested in other trials, which could be attributed to the significantly higher depth of cut, and thus more bond contact.

Wheel wear tests were conducted with dressing and grinding parameters shown in Tab. 11 and Tab. 14, respectively. The grinding parameters were suitable for creep feed grinding, considering  $Aggr=1.2 \cdot 10^{-5}$ . The wheel also had a more open structure and lower grit concentration allowing such a process without causing thermal damage on the workpieces.

**Tab. 14.** Grinding parameters for evaluating wheel wear with different grit sizes.

<b>Wheel speed, <math>v_s</math></b>	60 m/s
<b>Depth of cut, <math>a_e</math></b>	1 mm
<b>Workpiece speed, <math>v_w</math></b>	0.75 m/min
<b>Specific material removal rate, <math>Q'</math></b>	12.5 mm <sup>3</sup> /mm·s
<b>Aggressiveness, <math>Aggr</math></b>	1.20·10 <sup>-5</sup>
<b>Total volume removed,</b>	36, 24 and 12 cm <sup>3</sup> /mm

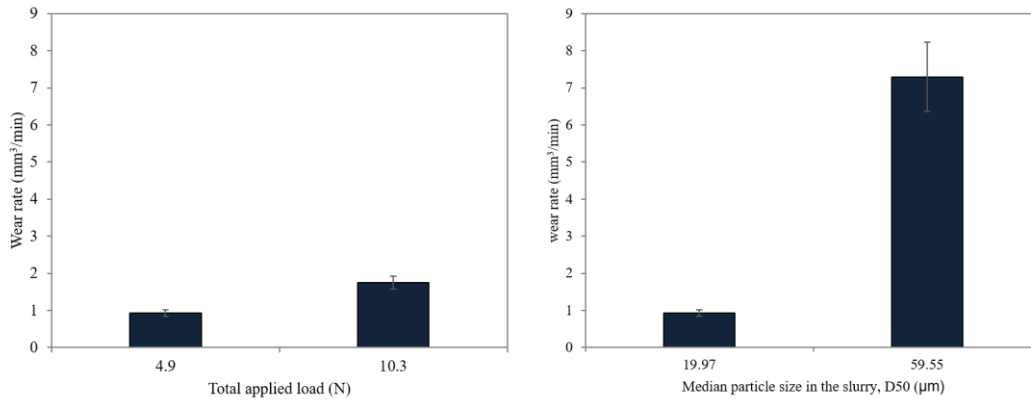
Fig. 33. shows that lower grinding wheel wear (higher G-ratio) is generated with wheels containing larger grits. This is accompanied by higher grinding forces. The opposite is true for smaller grits where higher wear (lower G-ratio) is observed, but the grinding forces are lower. Considering that the same grinding parameters were used, the process was less aggressive on the larger grit, which is less likely to fracture. Smaller grits, however, were subjected to harsher conditions and encountered more wear. Similarly, the dressing conditions potentially contributed to this phenomenon. The same dressing conditions can naturally generate a flatter area on the larger grit compared to the smaller grit. Larger wear flat area requires higher forces to fracture the grit, decreasing the wear process.



**Fig. 33.** G-ratio (grinding wheel wear) for wheels with different grit sizes.

### 3.5 Wear rate in accelerated tests using lapping-based test method

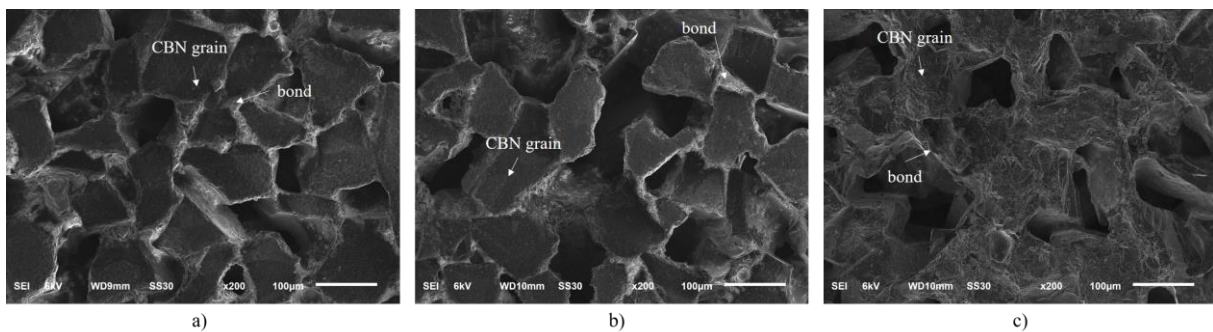
Preliminary tests were conducted to find the parameters that accelerate the wear rate without masking the effect of the grit-bond combination. The first test was carried out to compare the wear rate and the wear mechanisms when a load was applied (see Fig. 34a). The results show that the wear rate increases two-folds for 1.8N of additional axial load per sample. The wear rates for two sizes of diamond grits in the slurry (Fig. 34b) were also investigated. Here, we notice that the rate was approximately 7x larger when using a larger diamond size in the slurry.



**Fig. 34.** Lapping test with varying a) load applied normally to samples and b) average diamond grit size in the slurry.

Evaluation of lapped samples under Scanning Electron Microscope (SEM) highlighted that the micro-chipping was the dominant wear mode when changing the applied load (see Fig. 35), particularly on the top surface. Chang and Dornfeld [9] described that these ‘discrete indentations’ are typical for three body material removal mechanism. Trezona et al. [10] explained such surfaces are typical when the applied load is low, and the slurry concentration is high. However, it is interesting to note that the higher imposed load was sufficient to affect the weakest parts of the grit and bond, i.e. more damage on the edges of cBN grits and more bond fracture, as shown in Fig. 35b.

The situation changed when the diamond size in the slurry was increased. Under such conditions, the dominant wear mode was macro-chipping across the whole surface, as shown in the SEM images, see Fig. 35c. In addition, a considerable increase in bond breakage, bond wear and grain pull-out can be observed.



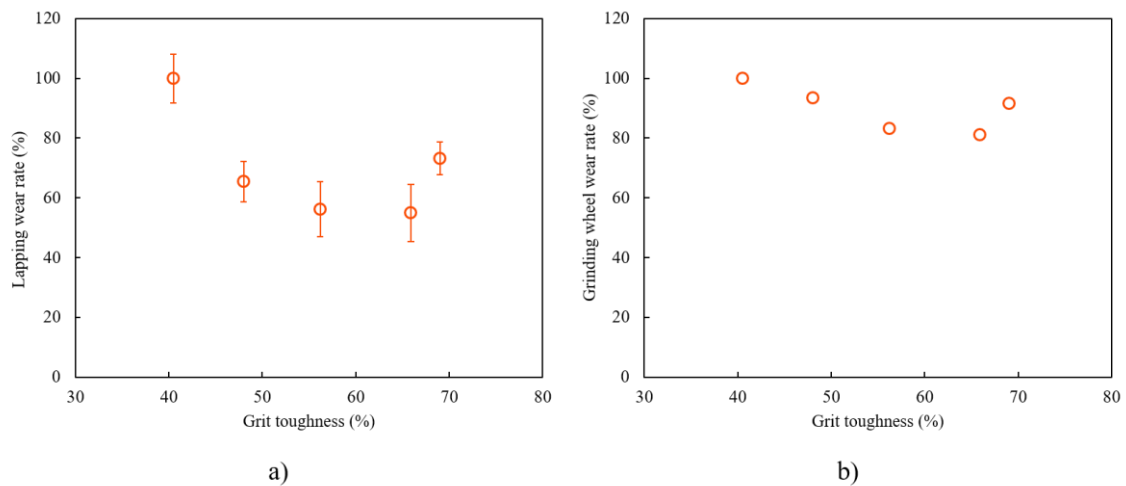
**Fig. 35.** SEM images of lapped samples subjected to a) 1.6N load and 10μm average diamond slurry size, b) 3.4N load and 10μm average diamond slurry size and c) 1.6N load and 59.55μm average diamond slurry size [70].

Based on this initial evaluation, the parameters to accelerate the wear rate, without masking the effect of the grit-bond combination, can be achieved by increasing the weight on the samples or the speed of rotation and keeping the grit size in the slurry below a certain limit.

### 3.5.1 Wear trends observed in lapping and grinding trials

The main focus was to investigate if the lapping method is sensitive enough to differentiate between different combinations of grit-bond systems. Here the focus was on cBN segments with different grit toughness ( $TI$ ). A comparison was made with cylindrical grinding because the same cBN-bond compositions were used in grinding wheels. More information, particularly on segments with various grit aspect ratios, can be found in Paper IV.

The effect of grit toughness on wear rate in lapping tests is shown in Fig. 36a. The results in both graphs were normalised with respect to the highest values. As expected, the wear rate decreases as grit toughness increases. However, the grit with the highest toughness saw a reversal, with an increase in wear. Similar trends are observed when using grits with different toughness in cylindrical grinding (see Fig. 36b). Once again, wear decreased with increasing the grit toughness. A similar observation was previously reported by Upadhyaya and Fiecoat [74]. However, the most interesting observation here is that the wear increases for the toughest grit, suggesting the result shown in lapping was most likely not an anomaly. The cause is difficult to ascertain, but a similar phenomenon, termed “wheel collapse” by Badger [21], can be considered. Collapse describes the lack of steady grit-fracture and bond-fracture, leading to excessive attritious wear followed by large-scale macro wear due to the large forces acting on the grit-bond system. Hence tougher grits require a suitable pairing in the grit-bond system, particularly considering higher aggressiveness.

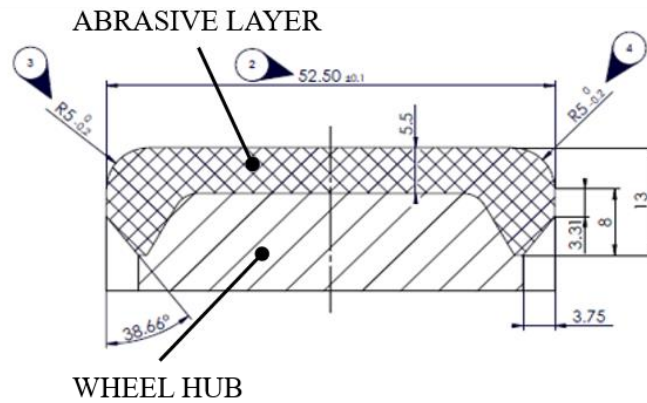


**Fig. 36.** Normalised wear rates for a) lapping-based method and b) cylindrical grinding tests [70].

### 3.6 Crankshaft grinding wheel design

Grinding wheels for crankshaft grinding applications usually have larger diameters to increase tool life and account for the eccentricity of the crankpins. In the case of Scania, the wheel has a diameter of 700mm. The shape of the abrasive layer corresponds to the pin shape in terms of radius sizes but with slightly narrower wheel width (see Fig. 37).

The reference grinding wheel, used at Scania, was a Tyrolit GENIS 2 wheel with a homogeneous layer of vitrified bonded B151 (ANSI 100120) grit and concentration of 160 (7 ct/cm<sup>3</sup> or 40% of the total matrix volume) (see Fig. 37). For the trials, E6 provided (the ABN800 grits) and Tyrolit produced the wheel.



**Fig. 37.** Technical drawing of a crankpin grinding wheel abrasive layer used in the crankshaft grinding by Scania.

### 3.7 Grinding wheel prototypes

Two wheels were prototypes produced by combining the knowledge of crankpin grinding challenges and understanding the effects of grits and wheel properties on grinding performance. The two main objectives were the reduction of heat and uneven wheel wear. Hence one wheel was focused on reducing uneven wheel wear, while the other was on reducing heat generation.

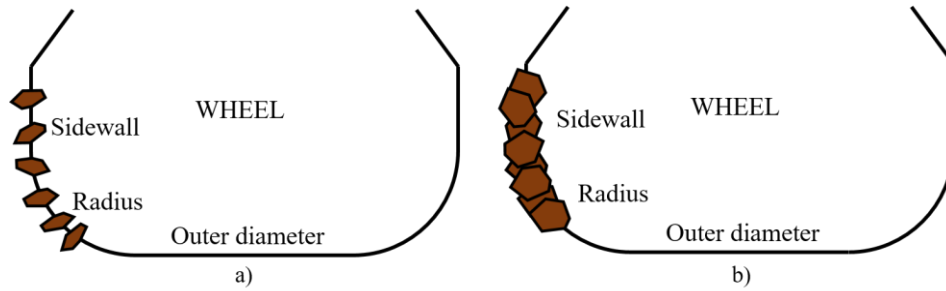
The following learnings (see previous sections) were guiding the wheel development:

- Grit aspect ratio and concentration affect grinding performance similarly; elongated grits and wheels with lower concentration exhibit lower intrinsic specific grinding energy  $e^*$  (they have higher protrusion) and lower sliding component of tangential stress  $\tau_0$ . However, in wear tests they show faster wear rate. The opposite is true for blocky grits and wheels with higher concentration, which generate higher  $e^*$  due to poorer grit exposure. Additionally, they generate higher  $\tau_0$  due to higher percent of wear flat area  $A$ . In the wear trials, however, they exhibit less wear.
- Wheels with larger grit size generate, similarly to blocky grits, higher sliding component of tangential stress  $\tau_0$  due to larger percent of wheel wear flat area  $A$ . At the same time, they exhibit lower intrinsic specific grinding energy  $e^*$  due to higher grit protrusion.

Smaller grits, on the other hand have lower  $\tau_0$  and higher  $e^*$  (lower grinding efficiency). Grinding wheel wear is higher for smaller grits.

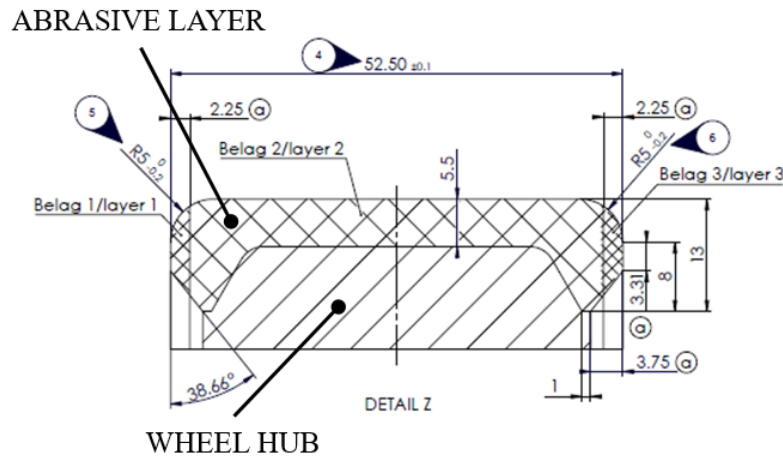
- Grit toughness  $TI$  and thermal stability  $TS$  affect the percent of wear-flat area  $A$  and the overall grit protrusion  $e^*$  at the same dressing conditions, causing different wheel performance. Similarly,  $TI$  and  $TS$  affect the wheel wear, which is generally higher if grits are weaker and less thermally stable.

Therefore, smaller and elongated grits at lower concentration were adopted to address heat generation challenges (see Fig. 38a), whereas larger, blockier grits at higher concentration were considered to tackle wheel wear (see Fig. 38b).



**Fig. 38.** a) Wheel design for reduction of grinding wheel wear and b) for reduction of heat generation.

The prototype wheels were produced with the same macro-geometry as the reference wheel. However, the abrasive layer, in this case, consisted of two layers (see Fig. 39): (i) the middle layer covering the outer diameter of the wheel and half of the radius (layer 2), (ii) side wall and the other half of the radius (layers 1 and 3). The layer composition of each wheel is summarized in Tab. 15.



**Fig. 39.** Newly developed grinding wheel with the middle abrasive layer equal to reference grinding wheel matrix. The two sides consist of customised layers.

**Tab. 15.** Layer compositions of three grinding wheels tested in production.

	<b>Composition description</b>	<b>Labelling on graphs and in the further sections</b>
<b>Reference wheel</b>	The whole profile consists of a homogeneous abrasive layer containing ABN800 ( $TI=49$ , $AR=1.48$ ) in size B151 with a concentration of 160.	ABN800 or reference wheel
<b>Prototype wheel 1</b>	Layer 2 has the same composition as the Reference wheel Layers 1 and 3 contain blockier grit ( $TI=70.1$ , $AR=1.32$ ) in size B181 and higher concentration than the reference wheel.	Wheel 1 or (B181, blocky, high C)
<b>Prototype wheel 2</b>	Layer 2 has the same composition as the Reference wheel Layers 1 and 3 contain elongated grit ( $TI=59.2$ , $AR=1.66$ ) in size B126 and lower concentration than the reference wheel.	Wheel 2 or (B126, elongated, low C)

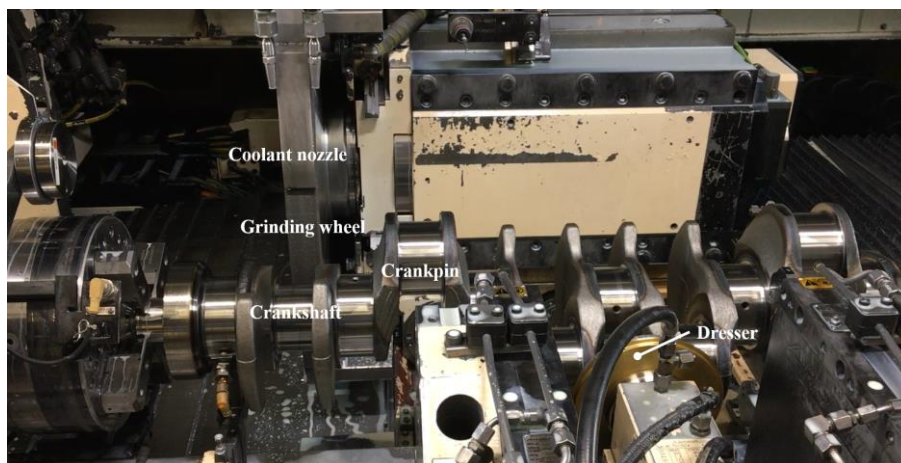
## 4 Production trials

### 4.1 Test setup

Crankshaft grinding trials were conducted in real production environment at Scania CV AB in Södertälje, Sweden. The two prototype wheels were tested alongside the reference wheel and their performance was compared. Workpieces were heavy-duty crankshafts with six crankpins (Fig. 40) made of low-alloy carbon steel. A Junker JUCRANK crankshaft grinding machine was used for all grinding trials. The grinding setup is presented in Fig. 41. The wheels ground six pins on each crankshaft, which are the most challenging parts to grind.



**Fig. 40.** Crankshaft with labelled crankpins were the focus parts in the grinding process.

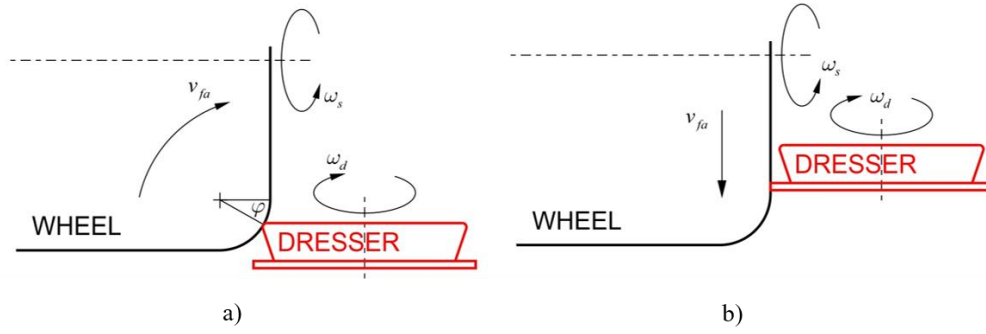


**Fig. 41.** Crankshaft grinding setup.

The dressing was carried out across the grinding wheel profile with two different dressing discs, typically used in Junker machines. The standard type rotary dresser was used to sharpen the grinding wheel's side wall and the cup wheel to sharpen the grinding wheel radius and outer diameter (Fig. 42). The dressing parameters for each portion of the wheel are summarised in

Tab. 16.





**Fig. 42.** Dressing set up standard for Junker crankshaft grinding machine [4].

**Tab. 16.** Dressing conditions used for trials.

	<b>Diameter and radius</b>	<b>Sidewall</b>
<b>Dressing depth, <math>a_d</math></b>	0.003mm	0.003mm
<b>Traverse speed, <math>f_{ad}</math></b>	400 (OD) & 50 (radius) mm/min	400 mm/min
<b>Wheel speed, <math>v_s</math></b>	80 m/s	80 m/s
<b>Dresser speed, <math>v_d</math></b>	66m/s	68 m/s
<b>Number of passes</b>	5	5

The grinding process was done in two stages, rough grinding followed by finish grinding. The temperature-based grinding method [17], with variable infeed speeds (axial and radial feed increments), was employed to avoid overheating the workpiece sidewall (see Tab. 17). For each grinding test, 15 crankshafts were processed. Scania has previously defined this number as a suitable dressing interval to avoid the onset of thermal damage on the workpiece. The dressing interval was kept the same for all wheels tested to prevent any grinding disturbances.

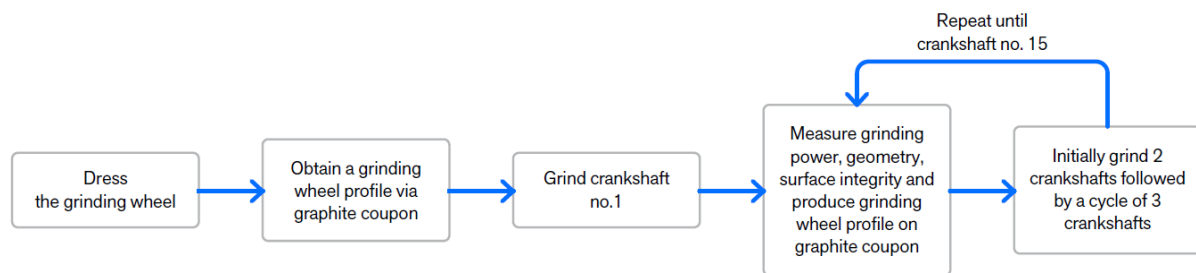
**Tab. 17.** Grinding conditions used for trials.

	<b>Rough grinding</b>	<b>Finish grinding</b>
<b>Workpiece RPM</b>	45	30-45
<b>Wheel speed</b>	48	45
<b>Grinding infeed</b>	11-27 $\mu\text{m}/\text{RPM}$	3-11 $\mu\text{m}/\text{RPM}$

## 4.2 Process evaluation


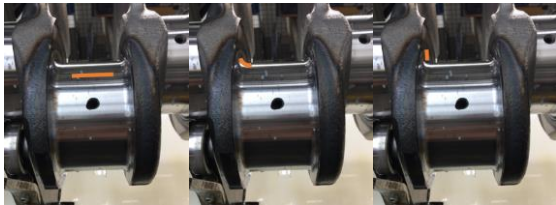

Quality assessment and analysis of workpieces and wheels were conducted to investigate any differences in wheel performance. The test protocol is shown in Fig. 43. Tab. 18 summarises the types of measurements and the measuring devices used.





**Fig. 43.** The test protocol, including measurement sequence.

**Tab. 18.** Measured features and measuring devices used in the trials.

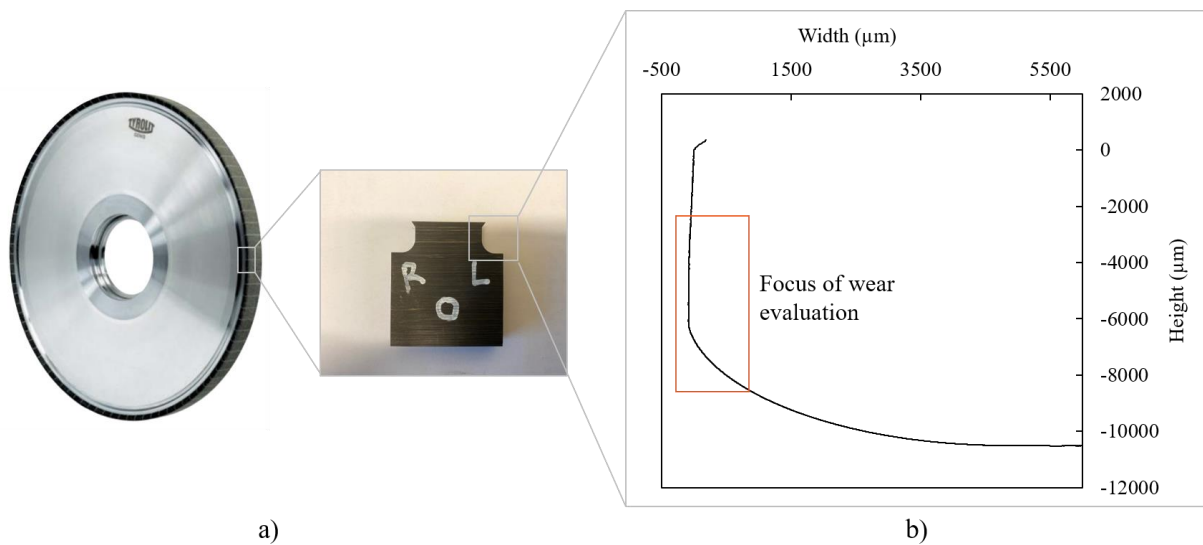
Measurements		Measuring device
Pin width		PFL air gauge
Surface roughness (on diameter, radius and side wall of crankpin)		Mahr surface measurement device
Barkhausen noise analysis- BNA		Rollscan R200 BN-signal analyser
Grinding wheel wear – graphite replica of the left and right side of the wheel		Alicona G5 Optical 3D Microscope
Power	Spindle power	NC- Fanuc servo guide

Surface roughness measurements were obtained using a Mahr device with customised setup, which allowed measuring roughness on all parts of the crankpin, i.e. diameter, radius and sidewall. Measurements were done on every measured crankshaft's first crankpin (see Fig. 40). Six measurements were taken across the profile of the crankpin, one on each sidewall and radii and two on the diameter. Roughness parameters relevant to different crankpin parts were measured. Ra was estimated on all parts as it is a good general description of height variations, although it is not sensitive to small changes in profile. Rz was measured on the diameter and the sidewall giving more information on high peaks and valleys. Rmax, measured on all three parts of the crankpin, focuses on determining the highest vertical distance between the Rp

(highest peak along the measured distance) and  $R_v$  (deepest valley- scratch- along the measured distance) [75].

Barkhausen noise, a non-destructive method for quantifying the surface integrity, was conducted with a Rollscan R200 BN-signal analyser. A wide-band sensor was used to analyse the signal in the 70–200 kHz frequency range. 159 measurements were obtained for each pin with a frequency angle of  $2.3^\circ$  (equally distributed around the circumference of each ground surface), and the average value was extracted.

The grinding wheel profiles were measured using the Alicona G5 via a graphite coupon (Fig. 44). Seven profiles were obtained as defined in the test protocol (see Fig. 43). Left and right sides of the grinding wheel sidewalls and radii were captured. The profiles obtained throughout the dressing interval were compared to evaluate the grinding wheel wear.

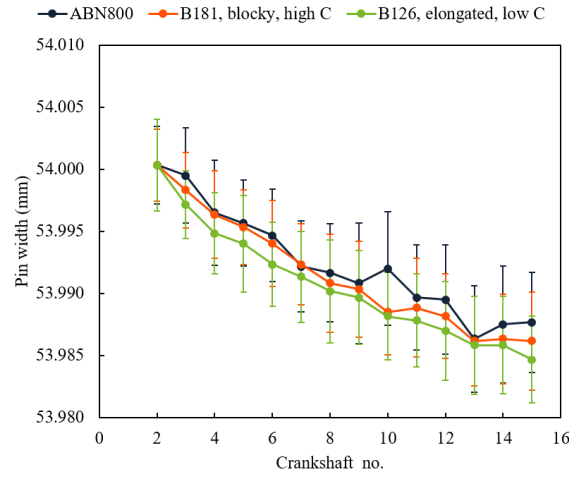


**Fig. 44.** Capturing grinding wheel wear: a) the grinding wheel is plunged into the graphite coupon. b) The coupon is imaged with the Alicona G5 to obtain a geometrical profile.

Spindle power was also measured throughout the cycle for rough- and finish-grinding. It is important to stress that it is impossible to separate the three features of the crankpin grinding (bearing surface, radius, sidewall) as the total power curve contains all contributions as all crankpin features are ground simultaneously.

### 4.3 Results and discussion

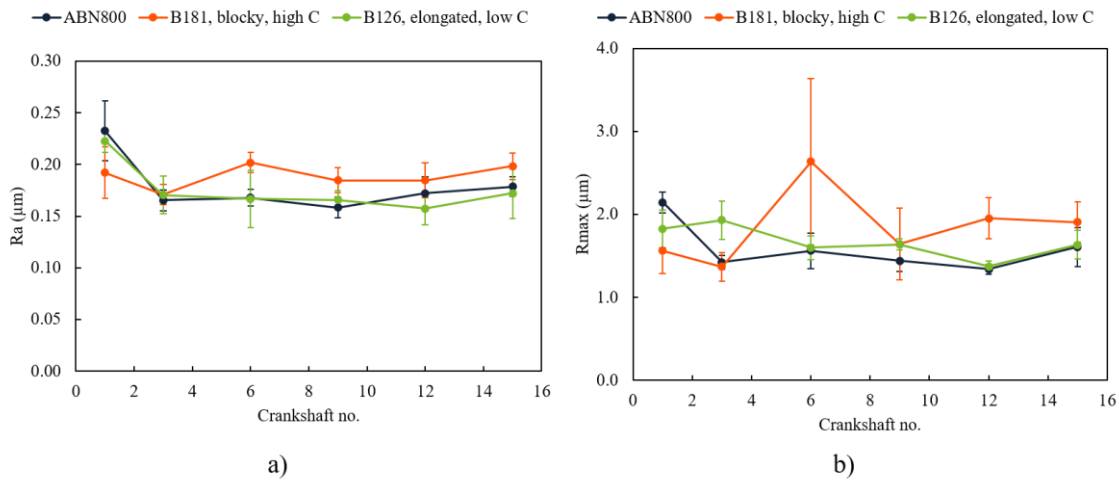
Pin width changes through the dressing interval for the reference and two prototype wheels are summarised in Fig. 45. Every point on the graph represents an average of six measured pins on the same crankshafts, while the error bars represent the standard deviation. The trends are comparable for the three-wheel designs, suggesting that the wear of grinding wheels affecting the crankpin width is similar.



**Fig. 45.** Pin width changes when using three different wheel designs.

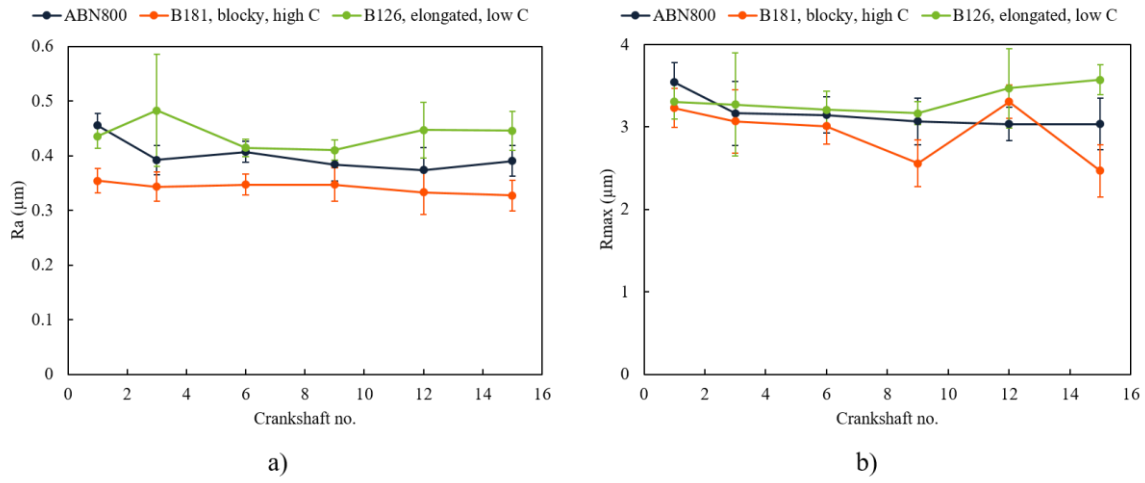
Surface roughness measurements of the crankpins were divided into three parts; the ones measured on the side wall (see Fig. 46), radius (see Fig. 47) and diameter (see Fig. 48). Even though the values were extracted from the left and right side of the crankpin (sidewall, radius and diameter), average values for each section are presented here with the standard deviation.

Roughness values on the side wall (Fig. 46) were expected to be the most different, considering it is the only portion of the pin affected by customised wheel design. The hypothesis was that the wheel with the blockiest grit and highest concentration would produce the best surface finish. However, Fig. 46 shows that the differences between the three wheel designs are insignificant. These results indicate that the large contact length and low aggressiveness on the sidewall have a first-order effect on the surface roughness. Thus, regardless of the type of grit used, the roughness is controlled by the severe rubbing process at this section of the pin. Also, note that the value of Ra on the side wall is two times smaller [0.15-0.20  $\mu\text{m}$ ] compared to the values on the radius and diameter, confirming that the rubbing process dominates this section.

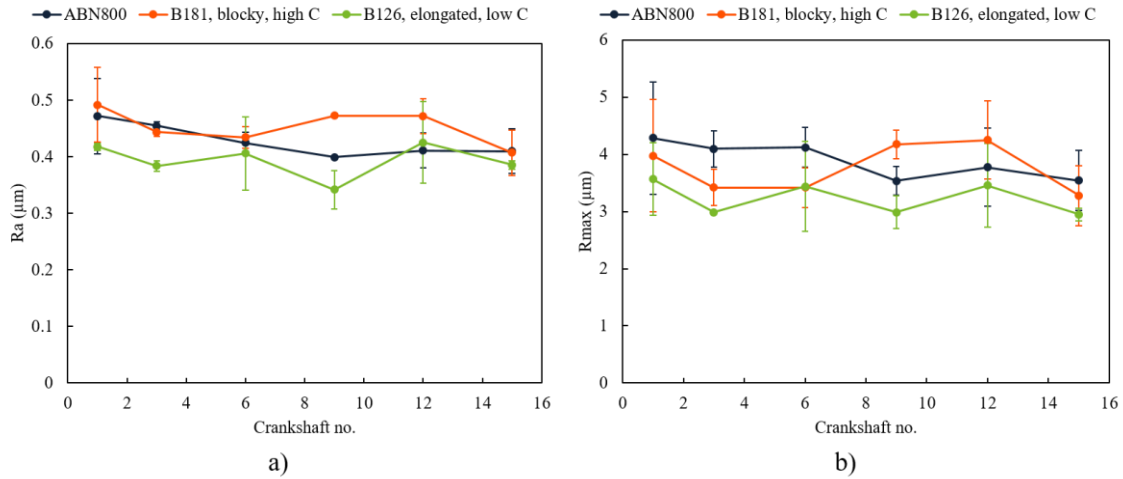


**Fig. 46.** Surface roughness parameters measured on the sidewall of the pins: a) Ra and b) Rmax.

Roughness on the radius (Fig. 47) and diameter (Fig. 48) is defined by the portion of the wheel that contains reference wheel design (ABN800), meaning that the differences observed on graphs are the result of process variations rather than the grinding wheel design.



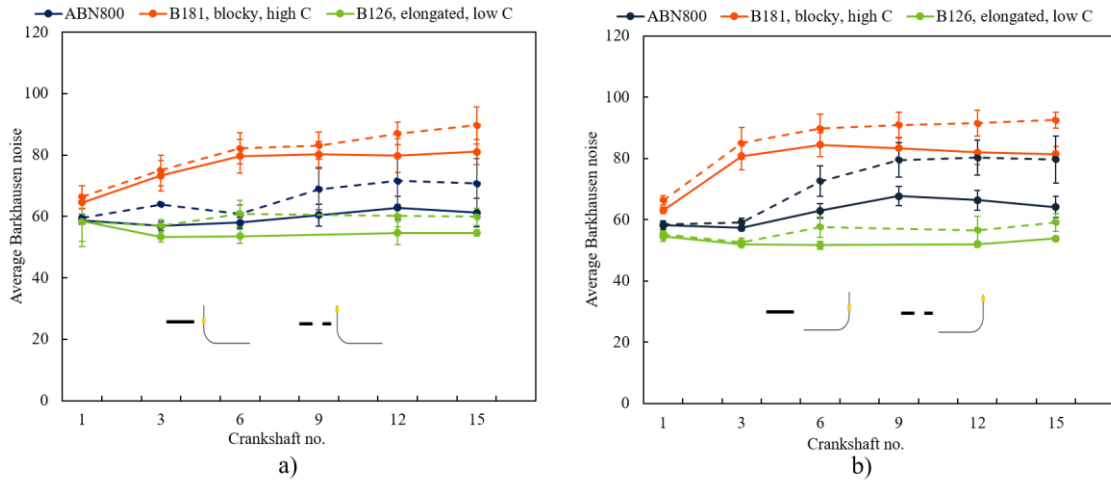
**Fig. 47.** Surface roughness measurements on the radius of the crankpin: a) Ra and b) Rmax.



**Fig. 48.** Surface roughness measurements on the crankpin's diameter (bearing surface): a) Ra and b) Rmax.

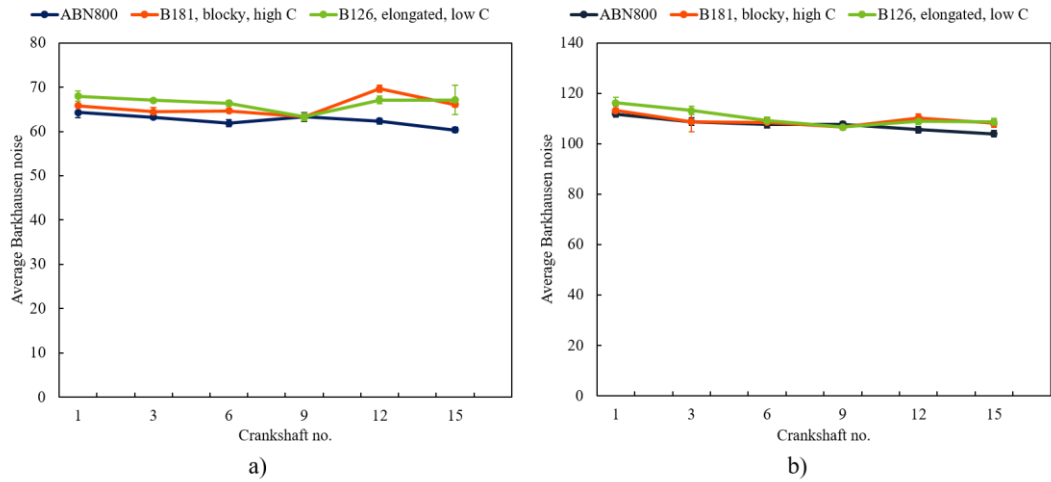
Similarly to roughness measurements, a hypothesis for Barkhausen noise values was that the most affected part on the crankpin would be the sidewall, where the wheel design is customised. Fig. 49 shows an average measurement of six pins for a particular crankshaft in the dressing interval and the standard deviation. Two measurements were conducted per crankpin; the first was close to the radius, and the second was higher on the side wall. The difference in results is up to 30% between the two different wheel designs on both sides of the crankpin. Wheel 1 (B181, blocky, high C) consistently generates higher Barkhausen noise measurements. The difference becomes particularly obvious after three ground crankshafts, which is relatively early in the dressing interval. The Barkhausen noise values stay consistently low throughout the

dressing interval for Wheel 2 (B126, elongated, low C), suggesting that Wheel 2 generates less contact between the wheel and the workpiece and, thus, more chip formation. On the other side, Wheel 1 (B181, blocky, high C) produces more contact, i.e. more prone to rubbing at the interface. The values of Barkhausen noise generally correlate with the workpiece's heat generation. The higher the Barkhausen noise levels, the more likely the workpiece has encountered higher temperatures, which can lead to thermal damage and, consequently, workpiece scrapping. The reference wheel sits between the two prototypes, which is expected considering that the grit concentration, grit size and shape of this wheel are between Wheel 1 (B181, blocky, high C) and Wheel 2 (B126, elongated, low C).



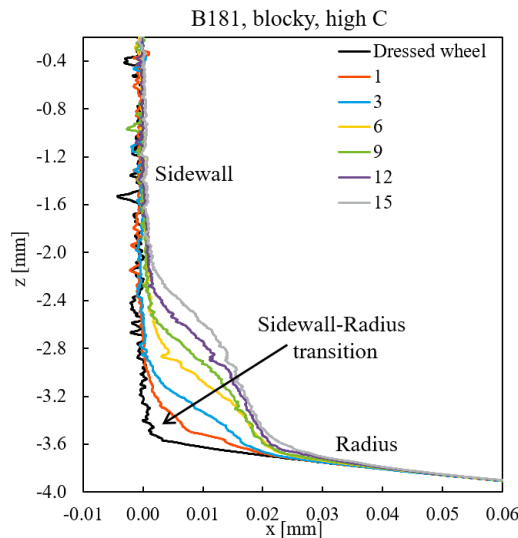
**Fig. 49.** Barkhausen noise values for the sidewall measured on two parts, closer to the radius and higher on the side wall for a) the left and b) the right side of the pin.

The radius and OD bearing surfaces on the crankpins are ground by the part of the wheel containing the reference grits, suggesting that minimal differences are expected here, Fig. 50 tends to confirm this hypothesis. The differences between customised wheel designs for radius and diameter on both sides are minimal. Because similar observations were made on the left and right sides of the part, only the results for the right side of the pin are presented. It is worth highlighting that the Barkhausen noise values vary between sections due to the geometry of the crankpin. Therefore, only measurements from a particular section of the crankpin should be compared.



**Fig. 50.** Barkhausen noise values measured on the a) radius and b) right side of the diameter (bearing surface).

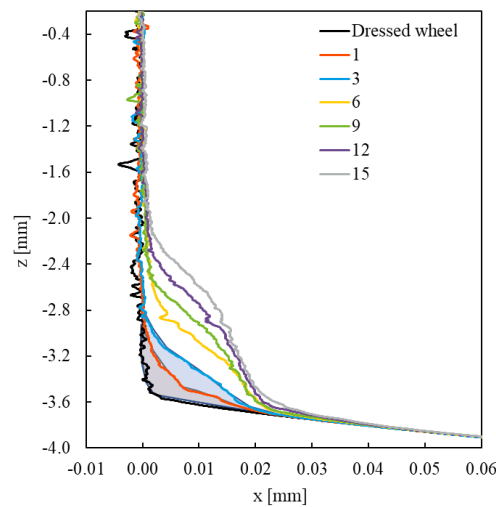
Grinding wheel wear progression was measured for the left and right sides of the grinding wheels, see Fig. 51 for the right side of Wheel 1. Each colour provides a profile after grinding a specific number of crankshafts, as shown in the legend; black is the profile of the dressed wheel, and grey is the profile of the wheel after grinding 15 crankshafts. It is not straightforward to determine where on the profile the wear started, considering that after only one ground crankshaft, the wear has already spread to the radius and sidewall. However, it is most likely, that the wear initially started on the radius close to the sidewall-radius transition and then spread to both adjacent areas.



**Fig. 51.** Wear progression of crankpin grinding wheel. The numbers in the legend represent the number of ground crankshafts.

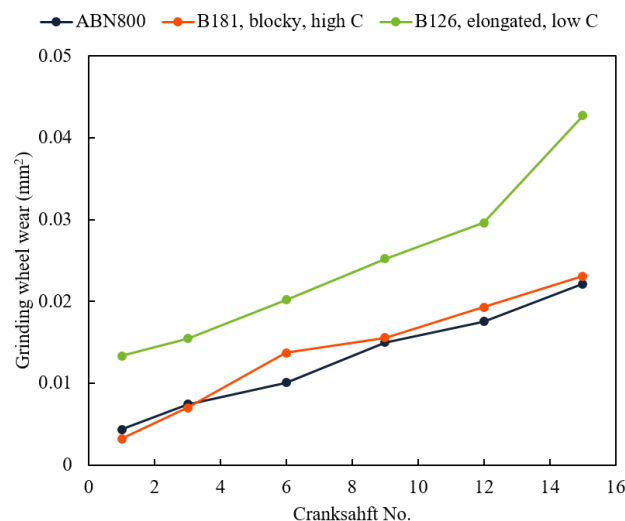
The grinding wheel wear comparison was made by measuring the differences in areas between the profiles as indicated in Fig. 52. The light orange area represents the difference between

dressed wheel and wheel after grinding the first crankshaft, etc. The area increase was then correlated to wheel wear.



**Fig. 52.** Measurement of wear via the difference in areas between profiles.

Fig. 53 shows that the wear rate is comparable for the three grinding wheels until crankshaft 12. After that, Wheel 2 (B126, elongated, low C) starts wearing faster while the other two wheels continue at the same rate. The most significant difference between the wheels is wear just after dressing, where Wheel 2 shows to be more affected than the reference (ABN800) wheel and Wheel 1 (B181, blocky, high C). This suggests that the same dressing conditions make Wheel 1 more prone to fracture due to grit and wheel properties. Surprisingly, there is no observable difference in wear progression between the reference wheel and Wheel 1, despite higher concentration and larger and blockier grits in the latter wheel.



**Fig. 53.** Wear progression for three tested grinding wheels.

The results from production trials indicate that in terms of heat reduction based on Barkhausen noise measurements, using smaller, elongated grits and a lower concentration wheel is preferable. However, in absolute terms, this grinding wheel wears faster, which is primarily affected by the dressing process. Surprisingly, the most suitable wheel to reduce the grinding wheel wear is the reference wheel, which produced a comparable amount of wear as Wheel 1 (B181, blocky, high C) but at lower Barkhausen noise levels.



## 5 Summary and future work

The main objective of the thesis was to develop a grinding wheel that would increase the dressing interval of the crankshaft grinding process. To achieve this, a collaborative project with the whole technology value chain (grit and wheel manufacturers, end-user) was established. This consortium was able to set realistic requirements specifications and was able to customise and experimentally try out an arbitrary bonded-abrasive tool. This was a rare example of research where an abrasive grit was customised and bonded into a prototype tool.

A dedicated experimental work was carried out to explore the performance variation using various wheel designs (1<sup>st</sup> research question). Different grits properties were evaluated with three types of tests. The first one focused on performance with negligible wear. To scientifically assess the performance of wheels during these tests, a novel analytical assessment framework was developed – bringing together established grinding mechanisms such as Malkin’s force models with a fundamental unifying measure of process geometry and kinematics bundled in the aggressiveness number. This framework can account for the effects of grit properties and dressing conditions on the wheel topography and, in turn, grinding performance. Such information is normally not available when using more established grinding-performance measures such as the characteristic specific grinding energy curve plotted against aggressiveness number, which fully accounts for process geometry and kinematics but does not explicitly consider surface-topography effects. The framework is applicable to a grinding regime that is dominated by cutting, with limited portions of rubbing and ploughing. In such a regime, which requires a certain (threshold) aggressiveness, a plot of  $\tau$  versus  $Aggr$  should yield a straight line whose slope is proportional to intrinsic specific grinding energy  $e^*$ , meaning that the correlation between tangential and normal stress is linear. It is further demonstrated that  $e^*$  is sensitive enough to distinguish between different grit protrusions, while the sliding component of tangential stress  $\tau_0$  fundamentally captures the percent of wheel wear-flat area. Additional contact between the wheel and the workpiece when grinding with a dull wheel is further captured via the friction coefficient  $\mu$  and the cutting efficiency with the force inclination  $\xi$ . The friction coefficient  $\mu$  depends on a combination of different rubbing actions at the interface and is affected by dressing conditions and grit properties; therefore,  $\mu$  is also a good indicator of cutting efficiency.

To complement the grinding performance of various wheels, the wear rate was evaluated using two different methods. The important conclusions of all conducted tests and the related 2<sup>nd</sup> research question are as follows:

- Grit aspect ratio and concentration affect grinding performance similarly; elongated grits and wheels with lower concentration exhibit lower intrinsic specific grinding energy  $e^*$  (they have higher protrusion) and a lower sliding component of tangential stress  $\tau_0$ . However, in wear tests, they show faster wear rate. The opposite is true for blocky grits and wheels with higher concentration, which generate higher  $e^*$  due to

poorer grit exposure. Additionally, they generate higher  $\tau_0$  due to higher wear flat area  $A$ . In the wear tests, however, they exhibit less wear.

- Wheels with larger grit size generate, similarly to blocky grits, a higher sliding component of tangential stress  $\tau_0$  due to larger percent of wheel wear flat area  $A$ . At the same time, they exhibit lower intrinsic specific grinding energy  $e^*$  due to higher grit protrusion. Smaller grits, on the other hand, have lower  $\tau_0$  and higher  $e^*$  (lower grinding efficiency). Grinding wheel wear is higher for smaller grits.
- Grit toughness  $TI$  and thermal stability  $TS$  affect the percent of wear flat area  $A$  and the overall grit protrusion  $e^*$  at the same dressing conditions, causing different wheel performance. Similarly,  $TI$  and  $TS$  affect the wheel wear, which is generally higher if grits are weaker and less thermally stable.
- Dressing conditions also affect wheel performance. Intrinsic specific grinding energy  $e^*$  and the sliding component of tangential stress  $\tau_0$  increase when wheels are dressed "duller", i.e. with a lower dressing aggressiveness  $Aggr_D$ . When the wheels are dressed "sharp", the window of operating grinding conditions gets wider due to lower  $e^*$ , primarily affected by the grit protrusion and lower  $\tau_0$  affected by the percent of wear-flat area  $A$ .

Based on understanding the crankshaft grinding challenges and outcomes of wheels performance testing, it was possible to design grinding wheels that would improve a real industrial grinding application (3<sup>rd</sup> research question). The first design (Wheel 1) focused on reducing grinding wheel wear, while the second (Wheel 2) on reducing heat generation.

## 5.1 Proposed solution and suggestions for future work

Production grinding trials conducted by the end-user have confirmed the predicted performance. Overall, Wheel 2 reduced heat generation, indicated by Barkhausen noise measurements, which showed a 20% reduction in intensity compared to the reference wheel and 30% reduction in intensity compared to the wheel design containing blockier and larger grit at higher concentration. Additionally, the Barkhausen noise measurements for Wheel 2 were constant throughout the dressing interval.

The next important step would be to do an extended test using Wheel 2 to determine the number of crankshafts ground by the time critical wear is reached. To complement this, it would also be essential to understand how much dressing would be required to remove 'excessive' grinding wheel wear. It is known that the dressing process directly relates to tool cost and that the end-users typically dress more than necessary to be on the safe side to achieve a more robust process.

Since Wheel 2, caused 10% higher Barkhausen noise levels on the sidewall compared to the reference wheel, it is likely this would require more frequent dressing as well. The dressing process is not productive. Even though dressing would not have to be substantial, if done frequently, it could result in similarly high tool cost and less time spent on grinding. This is

another reason that the wheel generating more efficient/free-cutting grinding is the preferable option.

Lastly, it would be beneficial to be able to predict wear behaviour by modelling the grinding wheel wear. This is, however, a very complex task considering all the variables.

## **5.2 Scientific contributions**

It is essential to highlight the contributions to the scientific and grinding community. Firstly, a novel analytical assessment framework can be used to evaluate grinding wheel performance that can account for the effects of grit properties and dressing conditions on the wheel topography and, in turn, grinding performance. Based on the classical Malkin and Cook model and aggressiveness number [55,76], a new set of new performance indicators are derived and then used to evaluate the effect of the wheel topography on the grinding process. The framework combined with experimental data can quantify how wheel wear flat area influences the sliding component and how grit protrusion influences the intrinsic specific grinding energy. Additional contact between the wheel and the workpiece can be further captured via the friction coefficient and the cutting efficiency with the force inclination. This framework provides a rational basis for evaluating grinding-wheel performance and abrasive-grit selection.

Secondly, a newly developed lapping-based method can capture the combined grit-bond system effects, as it can differentiate between several abrasive segments composed of cBN grits with different shapes (aspect ratio) and toughness when used with the same vitrified bond. Its primary benefits are short testing times and smaller specimen sizes. The lapping test could be used for screening purposes for both grit manufactures and abrasive-tool manufacturers wishing to reduce time-consuming grinding experiments.

As a consequence of collaborations, various customisations were possible, producing a unique bank of information, particularly regarding cBN grit properties and their effects on grinding performance, which can support the grinding community in the future. Lastly, a production challenge of crankpin grinding was addressed, based on wheel development and the performance was confirmed by the end-user trials.

## 6 Acknowledgements

Firstly, I would like to thank Element Six (UK) ltd. for funding and supporting my studies. Secondly, I would like to thank my boss and industrial supervisor Dr Luiz Franca, for his help, encouragement and his time. I appreciate all our discussions that thought me a great deal and helped solve numerous challenges. I want to extend the same gratitude to my main supervisor Professor Peter Krajnik who initially gave me the opportunity to work on the Crankshaft grinding challenges. Thank you for all your support and guidance throughout the studies. Thank you also to my co-supervisor Dr Radovan Drazumeric, for his input on technical challenges, discussions, modelling and insights in grinding and dressing processes.

Furthermore, I would like to thank several people and companies for their invaluable contributions:

- Roope Roininen for his technical input and for completing industrial grinding trials during the pandemic.
- Dr Markus Weiss, Tim Lorkowski, Jyrki Grindberg and Staffan Bentzer for their technical contributions and discussions throughout the project.
- Scania for time and resources to complete production trials in the midst of the pandemic.
- Tyrolit for producing grinding wheels throughout the project.
- Element Six (UK) ltd for time and resources to complete numerous grinding trials and for manufacturing unique cBN grit types.
- Dr Maria Cann for proofreading the thesis.

Last but not least, I would like to express my love to my husband who has been my biggest cheerleader since the start. I am very grateful to have you in my life. Thank you also to my family and friends for their support.

## 7 References

- [1] F. Hashimoto, H. Yamaguchi, P. Krajnik, K. Wegener, R. Chaudhari, H.W. Hoffmeister, F. Kuster. Abrasive Fine-Finishing Technology. *CIRP Ann. - Manuf. Technol.* 2016; 65 (2): 597–620.
- [2] R. Dražumerič, R. Roininen, J. Badger, P. Krajnik. Temperature-Based Method for Determination of Feed Increments in Crankshaft Grinding. *J. Mater. Process. Technol.* 2018; 259 (April): 228–234.
- [3] P. Comley, I. Walton, T. Jin, D.J. Stephenson. A High Material Removal Rate Grinding Process for the Production of Automotive Crankshafts. *CIRP Ann.* 2006; 55 (1): 347–350.
- [4] R. Dražumerič, J. Badger, R. Roininen, P. Krajnik. On Geometry and Kinematics of Abrasive Processes: The Theory of Aggressiveness. *Int. J. Mach. Tools Manuf.* 2020; 154: 103567.
- [5] P. Krajnik, R. Drazumeric. Method of grinding a workpiece and method for determining processing parameters, European patent EP 3145672 A1, 2014.
- [6] V. Radhakrishnan, B.T. Achyutha. A Method for Reducing the Corner Wear in Plunge Grinding. *Proc. Inst. Mech. Eng. Part B Manag. Eng. Manuf.* 1986; 200: 19–26.
- [7] E. Junker. Rough-grinding and finish-grinding a crankshaft in a clamping, European Patent EP1181132 B1, 2003.
- [8] A. Watanabe. Grinding wheel, US 2017/0014972 A1, 2017.
- [9] I. Suzuki, Y. Oda. Method of grinding a workpiece having a cylindrical portion and shoulder portions, 4,603,514, 1986.
- [10] J.F.G. Oliveira, E.J. Silva, J.J.F. Gomes, F. Klocke, D. Friedrich. Analysis of Grinding Strategies Applied to Crankshaft Manufacturing. *CIRP Ann. - Manuf. Technol.* 2005; 54 (2): 269–272.
- [11] M. Banks, E.R. Randell, D.W. Hall, C.D. Bartlett, S. Clewes. Improvements in and relating to the grinding of cylindrical surfaces and adjoining side-walls, European patent EP 1635989 B1, 2007.
- [12] N. Itoh, A. Watanabe. Grinding method, US 2008/0311828A1, 2008.
- [13] S. Soma, H. Morita. Grinding method and grinding machine, US 7,530,882 B2, 2009.
- [14] J.C. Jaeger. Moving Sources of Heat and the Temperature of Sliding Contacts. *Proc. R. Soc. New South Wales* 1942; 76: 203–224.
- [15] J. Badger, R. Dražumeric, P. Krajnik. Application of the Dimensionless Aggressiveness Number in Abrasive Processes. *Procedia CIRP* 2021; 102: 361–368.
- [16] P. Krajnik, R. Drazumeric, J. Badger, R. Roininen. High-Performance Industrial Grinding: Recent Advances and Case Studies from the Automotive Engine Production, in: *Proc. 19th Int. Symp. Adv. Abras. Technol.*, 2016: pp. 1–13.
- [17] P. Krajnik, R. Roininen, R. Drazumeric. Method of grinding a workpiece having a cylindrical bearing surface and method for determining processing parameters, EP3115149B1, 2018.
- [18] K. Wegener, H.W. Hoffmeister, B. Karpuschewski, F. Kuster, W.C. Hahmann, M. Rabiey. Conditioning and Monitoring of Grinding Wheels. *CIRP Ann.* 2011; 60 (2): 757–777.
- [19] S. Malkin, T. Murray. Mechanics of Rotary Dressing of Grinding Wheels. *J. Eng. Ind.* 1978; 100 (1): 95–102.
- [20] T. Murray, S. Malkin. Effects of Rotary Dressing on Grinding Wheel Performance. *J. Eng. Ind.* 1978; 100 (3): 297–302.
- [21] E. Brinksmeier, M. Çinar. Characterization of Dressing Processes by Determination of the Collision Number of the Abrasive Grits. *CIRP Ann.* 1995; 44 (1): 299–304.

- [22] T. Ishikawa, K. V Kumar. Conditioning of vitrified bond superabrasive wheels, in: Proc. Conf. Super-Abrasives, Chicago, Illionis, 1991: p. 7.91-7.110.
- [23] M.C. Shaw. Principles of abrasive processing, Clarendon Press, 1996.
- [24] E. Saljé, H.G. v. Mackensen. Dressing of Conventional and CBN Grinding Wheels with Diamond Form Rollers. CIRP Ann. 1984; 33 (1): 205–209.
- [25] A. Spampinato, D.A. Axinte. On Modelling the Interaction between Two Rotating Bodies with Statistically Distributed Features: An Application to Dressing of Grinding Wheels. Proc. R. Soc. A. 2017; 437 (1–21):.
- [26] J. Yang, D.-Y. Kim, H.-Y. Kim. Effect of Glass Composition on the Strength of Vitreous Bonded C-BN Grinding Wheels. Ceram. Int. 1993; 19 (2): 87–92.
- [27] D. Shan, Z. Li, Y. Zhu, H. Ye, K. Gao, Y. Yu. Influence of TiO<sub>2</sub> on the Physical Properties of Low-Temperature Ceramic Vitrified Bond and Mechanical Properties of CBN Composites. Ceram. Int. 2012; 38 (6): 4573–4578.
- [28] J. Shi, F. He, J. Xie, X. Liu, H. Yang. Effect of Heat Treatments on the Li<sub>2</sub>O-Al<sub>2</sub>O<sub>3</sub>-SiO<sub>2</sub>-B<sub>2</sub>O<sub>3</sub>-BaO Glass-Ceramic Bond and the Glass-Ceramic Bond CBN Grinding Tools. Int. J. Refract. Met. Hard Mater. 2019; 78: 201–209.
- [29] X. Wang, T. Yu, X. Sun, Z. Wang, W. Wang. Effects of ZrO<sub>2</sub> on Physical and Mechanical Properties of Vitrified Bond CBN Composite Materials. J. Ceram. Process. Res. 2016; 17 (9): 969–973.
- [30] M.J. Jackson, B. Mills, M.P. Hitchiner. Controlled wear of vitrified abrasive materials for precision grinding applications, in: Sadhana Acad. Proc. Eng. Sci., 2003: pp. 897–914.
- [31] R. Cai, W.B. Rowe, M.N. Morgan. The Effect of Porosity on the Grinding Performance of Vitrified CBN Wheels. Key Eng. Mater. - KEY ENG MAT 2003; 238: 295--300.
- [32] X. Lv, Z. Li, Y. Zhu, J. Zhao, G. Zhao. Effect of PMMA Pore Former on Microstructure and Mechanical Properties of Vitrified Bond CBN Grinding Wheels. Ceram. Int. 2013; 39 (2): 1893–1899.
- [33] T. Tanaka, S. Edaki, T. Nishida, T. Nakajima, K. Ueno. Development and Application of Porous Vitrified-Bonded Wheel with UltraFine Diamond Abrasives. Key Eng. Mater. - KEY ENG MAT 2004; 257–258: 251–256.
- [34] J.B. Mao, F.L. Zhang, G.C. Liao, Y.M. Zhou, H.P. Huang, C.Y. Wang, S.H. Wu. Effect of Granulated Sugar as Pore Former on the Microstructure and Mechanical Properties of the Vitrified Bond Cubic Boron Nitride Grinding Wheels. Mater. Des. 2014; 60: 328–333.
- [35] X. Lv, Z. Li, Y. Zhu, J. Zhao, G. Zhao. Effect of PMMA Pore Former on Microstructure and Mechanical Properties of Vitrified Bond CBN Grinding Wheels. Ceram. Int. 2013; 39 (2): 1893–1899.
- [36] T.D. Davis, J. DiCorleto, D. Sheldon, J. Vecchiarelli, C. Erkey. A Route to Highly Porous Grinding Wheels by Selective Extraction of Pore Inducers with Dense Carbon Dioxide. J. Supercrit. Fluids 2004; 30 (3): 349–358.
- [37] W.F. Ding, J.H. Xu, Z.Z. Chen, C.Y. Yang, C.J. Song, Y.C. Fu. Fabrication and Performance of Porous Metal-Bonded CBN Grinding Wheels Using Alumina Bubble Particles as Pore-Forming Agents. Int. J. Adv. Manuf. Technol. 2013; 67 (5–8): 1309–1315.
- [38] R.H. Wentorf. Abrasive material and preparation thereof, US2947617, 1960.
- [39] S. Malkin, C. Guo. Grinding technology: theory and applications of machining with abrasives, in: Grind. Technol. Theory Appl. Mach. with Abrasives, 2nd ed., Industrial Press, New York, 2008: pp. 115–156.
- [40] N. Macerol, L. Franca, W. Leahy, P. Krajnik. Superabrasive Applications in Grinding of Crankshafts: A Review. ISAAT 2017 - Proc. 20th Int. Symp. Adv. Abras. Technol. 2017;

- 911–919.
- [41] M.J. Jackson, C.J. Davis, M.P. Hitchiner, B. Mills. High-Speed Grinding with CBN Grinding Wheels — Applications and Future Technology. *J. Mater. Process. Technol.* 2001; 110 (1): 78–88.
  - [42] G. Davies. Materials synthesis- internal report, 2014.
  - [43] B.A. Cooley. Superhard Abrasive Developments from De Beers, in: *Int. Congr. Diamonds Ind.*, 1976: pp. 17–29.
  - [44] O. Fukunaga, S. Nakano, T. Taniguchi. Nucleation and Growth of Cubic Boron Nitride Using a Ca-B-N Solvent. *Diam. Relat. Mater.* 2004; 13 (9): 1709–1713.
  - [45] T. Taniguchi, S. Yamaoka. Spontaneous Nucleation of Cubic Boron Nitride Single Crystal by Temperature Gradient Method under High Pressure. 2001; 222: 549–557.
  - [46] T. Taniguchi, S. Koizumi, K. Watanabe, I. Sakaguchi, T. Sekiguchi. High Pressure Synthesis of UV-Light Emitting Cubic Boron Nitride Single Crystals. 2003; 12: 1098–1102.
  - [47] Y. Kubota, T. Taniguchi. Synthesis of Cubic Boron Nitride Using Ni-Mo Alloy as a Solvent. *Jpn. J. Appl. Phys.* 2008; 47 (11): 8375–8378.
  - [48] Y. Ichida, M. Fujimoto, Y. Inoue, K. Matsui. Development of a High Performance Vitrified Grinding Wheel Using Ultrafine-Crystalline CBN Abrasive Grains. *J. Adv. Mech. Des. Syst. Manuf.* 2010; 4 (5): 1005–1014.
  - [49] B. Zhao, W. Ding, Y. Zhou, H. Su, J. Xu. Effect of Grain Wear on Material Removal Behaviour during Grinding of Ti-6Al-4V Titanium Alloy with Single Aggregated CBN Grain. *Ceram. Int.* 2019; 45 (12): 14842–14850.
  - [50] Z. Rao, W. Ding, Y. Zhu, H. Su. Understanding the Self-Sharpening Characteristics of Polycrystalline Cubic Boron Nitride Super-Abrasive in High-Speed Grinding of Inconel 718. *Ceram. Int.* 2019; 45 (10): 13324–13333.
  - [51] Y. Zhu, W. Ding, Z. Rao, C. Yang. Micro-Fracture Mechanism of Polycrystalline CBN Grain during Single Grain Scratching Tests Based on Fractal Dimension Analysis. *Precis. Eng.* 2019; 59: 26–36.
  - [52] M.W. Bailey, L.K. Hedges. Crystal morphology identification of diamond and ABN, in: *Ind. Diam. Rev.*, 1995: pp. 11–14.
  - [53] B.T. Achyutha, V. Radhakrishnan. A Study of the Corner Wear in Cylindrical Plunge Grinding. *Int. J. Mach. Tool Des. Res.* 1985; 25 (4): 287–297.
  - [54] K.& RIEDEL. Vittrified-bonded CBN and diamond tools from KREBS & RIEDEL. <https://www.krebs-riedel.de/DOC/KCE-101-2020.pdf> Acc: November 12, 2022.
  - [55] S. Malkin, N.H. Cook. The Wear of Grinding Wheels: Part 1—attritious Wear. *ASME. J. Eng. Ind.* 1971; 93 (4): 1120–1128.
  - [56] M.P. Hitchiner, S.B. Mcspadden. Evaluation of Factors Controlling CBN Abrasive Selection for Vittrified Bonded Wheels. *CIRP Ann. - Manuf. Technol.* 2005; (3): 3–6.
  - [57] J. Badger. Factors Affecting Wheel Collapse in Grinding. *CIRP Ann.* 2009; 58 (1): 307–310.
  - [58] Unified Abrasives Manufacturers' Association. For Measuring-Relative Crystal Strengths of Diamond and Cubic Boron Nitride Grit, ANSI B74.23-2002. 2002; .
  - [59] M.. Jackson, M.J., Mills, B. and Hitchiner. Controlled Wear of Vittrified Abrasive Materials for Precision Grinding Applications. *Sadhana* 2003; 28 (5): 897–914.
  - [60] K. Breder, N. Corbin, P. Chinnakaruppan, S. Hartline. The influence of grinding conditions on the performance of different CBN types, in: *Ind. Diam. Rev.*, 2005: pp. 4–7.
  - [61] N. Macerol, L.F.P. Franca, R. Drazumeric, P. Krajnik. The Effects of Grit Properties and Dressing on Grinding Mechanics and Wheel Performance: Analytical Assessment Framework. *Int. J. Mach. Tools Manuf.* 2022; 180 (July): 103919.

- [62] Y. Chen, X. Chen, L. Aiouarab, T. Opoz, X.P. Xu, G. Yu. Morphology Analysis and Characteristics Evaluation of Typical Super Abrasive Grits in Micron Scale. *J. Superhard Mater.* 2019; 41 (3): 189–200.
- [63] Federation of European Producers of Abrasives. FEPA Standards for Checking Superabrasives Grain Sizes, 2009 Edition, 61-2009. 2009; .
- [64] Unified Abrasives Manufacturer's Association. Checking the Size of Diamond or Cubic Boron Nitride Abrasive Products, ANSI B74.16:2002. 2002; .
- [65] Retsch Technology. Particle Size and Particle Shapeanalysis with Dynamic Image Analyser. 2015; 1–12.
- [66] R. Snoeys, J. Peters. The Significance of Chip Thickness in Grinding. *Ann. CIRP* 1974; 23: 227–237.
- [67] Glomacht- Global Machinery Trading. .
- [68] M. Mostofi. Drilling Repsponse of impregnated diamond bits: modelling and experimental investigation, Curtin University, 2014.
- [69] R.D. Monici, E.C. Bianchi, R.E. Catai, P.R. De Aguiar. Analysis of the Different Forms of Application and Types of Cutting Fluid Used in Plunge Cylindrical Grinding Using Conventional and Superabrasive CBN Grinding Wheels. *Int. J. Mach. Tools Manuf.* 2006; 46 (2): 122–131.
- [70] N. Macerol, L. Franca, H. Attia, P. Krajnik. A Lapping-Based Test Method to Investigate Wear Behaviour of Bonded-Abrasive Tools. *CIRP Ann.* 2022; 71 (1): 305–308.
- [71] Engineering ToolBox. Friction and friction coefficients. [https://www.engineeringtoolbox.com/friction-coefficients-d\\_778.html](https://www.engineeringtoolbox.com/friction-coefficients-d_778.html) Acc: November 27, 2022.
- [72] M.P. Hitchiner, S.B. McSpadden, J.A. Webster. Evaluation of Factors Controlling CBN Abrasive Selection for Vitrified Bonded Wheels. *CIRP Ann.* 2005; 54 (1): 277–280.
- [73] J. Badger, S. Murphy, G.E. O'Donnell. Big-and-Dull or Small-and-Sharp: A Comparison of Specific Energy, Wheel Wear, Surface-Generation Mechanisms and Surface Characteristics When Grinding with Al<sub>2</sub>O<sub>3</sub> and CBN to Achieve a given Surface Roughness. *J. Mater. Process. Technol.* 2021; 288: 116825.
- [74] R.P. Upadhyaya, J.H. Fiecoat. Factors Affecting Grinding Performance with Electroplated CBN Wheels. *CIRP Ann.* 2007; 56 (1): 339–342.
- [75] E.S. Gadelmawla, M.M. Koura, T.M.A. Maksoud, I.M. Elewa, H.H. Soliman. Roughness Parameters. *J. Mater. Process. Technol.* 2002; 123 (1): 133–145.
- [76] S. Malkin, N.H. Cook. The Wear of Grinding Wheels: Part 2—Fracture Wear. *ASME. J. Eng. Ind.* 1971; 93 (4): 1129–1133.